

1 High-resolution distributions of $\Delta(\text{O}_2/\text{Ar})$ on the northern slope of the
2 South China Sea and estimates of net community production

3 Chuan Qin^{1,2}, Guiling Zhang^{1,2,*}, Wenjing Zheng¹, Yu Han^{1,3}, Sumei Liu^{1,2}
4

5 1. Key Laboratory of Marine Chemistry Theory and Technology, Ministry of Education/Institute for
6 Advanced Ocean Study, Ocean University of China, 238 Songling Road, 266100 Qingdao, P. R.
7 China

8 2. Laboratory for Marine Ecology and Environmental Science, Qingdao National Laboratory for
9 Marine Science and Technology, Qingdao 266237, P. R. China

10 3. Hainan Tropical Ocean University, Sanya 572022, P. R. China

11 * Correspondence to: Guiling Zhang (guilingzhang@ouc.edu.cn)

12 **Abstract**

13 Dissolved oxygen-to-argon ratio (O_2/Ar) in the oceanic mixed layer has been widely used to
14 estimate net community production (NCP), which is the difference between gross primary
15 production and community respiration and is a measure for the strength of the biological pump.

16 In order to obtain the high-resolution distribution of NCP and improve our understanding of its
17 regulating factors in the slope region of the Northern South China Sea (SCS), we conducted

18 continuous measurements of dissolved O_2 , Ar, and CO_2 by membrane inlet mass spectrometry
19 (MIMS) during two cruises in October 2014 and June 2015. An overall autotrophic condition

20 was observed in the study region in both cruises with an average $\Delta(\text{O}_2/\text{Ar})$ of $1.1\% \pm 0.9\%$ in
21 October 2014 and $2.7\% \pm 2.8\%$ in June 2015. NCP was on average $11.5 \pm 8.7 \text{ mmol C m}^{-2} \text{ d}^{-1}$

22 in October 2014 and $11.6 \pm 12.7 \text{ mmol C m}^{-2} \text{ d}^{-1}$ in June 2015. Correlations between dissolved
23 inorganic nitrogen (DIN), $\Delta(\text{O}_2/\text{Ar})$, and NCP were observed in both cruises, indicating that

24 NCP is subject to the nitrogen limitation in the study region. In June 2015, we observed a rapid
25 response of the ecosystem to the episodic nutrient supply induced by eddies. Eddy-entrained

26 shelf water intrusion, which supplied large amounts of terrigenous nitrogen to the study region,
27 promoted NCP in the study region by potentially more than threefold. In addition, upwelling

28 brought large uncertainties to the estimation of NCP in the core region of the cold eddy (cyclone)
29 in June 2015. The deep euphotic depth in the SCS and the absence of correlation between NCP

30 and the average photosynthetically available radiation (PAR) in the mixed layer in the autumn

31 indicate that light availability may not be a significant limitation on NCP in the SCS. This study
32 helps to understand the carbon cycle in the highly dynamic shelf system.

33

34 **Keywords:** O₂/Ar; Net community production; Nutrients; Eddy; Northern slope of South China
35 Sea

36

37 **1. Introduction**

38 The oceanic carbon sequestration is partially regulated by the production and export
39 process of biological organic carbon in the surface ocean. Net community production
40 (NCP) corresponds to gross primary production (GPP) minus community respiration
41 (CR) in the water (Lockwood et al., 2012) and is an important indicator of carbon export.
42 At steady state, NCP is equivalent to the rate of organic carbon export, and is a measure
43 for the strength of the biological pump (Lockwood et al., 2012). NCP effectively
44 couples carbon cycle and oxygen (O₂) production through photosynthesis and
45 respiration in the euphotic layer, thus many previous researches measured the mass
46 balance of O₂ to quantify NCP (e.g., Emerson et al., 1991; Hendricks et al., 2004;
47 Huang et al., 2012; Reuer et al., 2007). Argon (Ar), a biological inert gas, was
48 commonly used to normalize the O₂ concentration in these researches. Based on the
49 similar solubility properties of O₂ and Ar, oxygen-to-argon ratio (O₂/Ar) can remove
50 the influences of physical processes (i.e., temperature and pressure change, bubble
51 injection) on the mass balance of O₂ (Craig and Hayward, 1987). Dissolved O₂/Ar has
52 been developed as a proxy for NCP in a water mass (Kaiser et al., 2005). The biological
53 production in the open oceans (i.e., Southern Ocean, Pacific, Arctic Ocean) has been
54 inferred using the O₂/Ar ratio to estimate NCP in numerous researches (e.g., Hamme et
55 al., 2012; Lockwood et al., 2012; Ulfsbo et al., 2014; Shadwick et al., 2015; Stanley et
56 al., 2010). During recent years, several high-resolution measurements of O₂/Ar and
57 NCP in coastal waters have been reported (Tortell et al., 2012; Tortell et al., 2014;
58 Eveleth et al., 2017; Izett et al., 2018). Despite the coastal waters such as shelves and
59 estuaries only accounting for 7 % of the global ocean surface area, they are known to

60 contribute to 15–30 % of the total oceanic primary production (Bi et al., 2013; Cai et
61 al., 2011) and play an important role in marine carbon cycle and production. However,
62 these regions still suffer from low resolution measurements that can't provide
63 representative high-resolution NCP data.

64 The South China Sea (SCS) is one of the largest marginal seas in the world with
65 complex ecological characteristics. River runoff from the Pearl and Mekong Rivers
66 introduces large amounts of dissolved nutrients into the SCS (Ning et al., 2004). Due
67 to the influence of seasonal monsoons, the surface circulation in the SCS changes from
68 a basin-scale cyclonic gyre in winter to an anticyclonic gyre in summer (Hu et al., 2000).
69 The surface water masses on the northern slope of SCS can be categorized into three
70 regimes: shelf water, offshore water (e.g., the intruded Kuroshio water), and the SCS
71 water (Feng, 1999; Li et al., 2018). The shelf water is mixed with fresh water from
72 rivers or coastal currents and thus usually has low salinity ($S < 33$) and low density (Uu
73 and Brankart, 1997; Su and Yuan, 2005; Cheng et al., 2014). Both offshore water and
74 SCS water originate from the Northern Pacific. Thus offshore water has similar
75 hydrographic characteristics of high temperature and high salinity as the Northern
76 Pacific water. But the SCS water has changed a lot in its hydrographic property because
77 of the mixing processes, heat exchange and precipitation during its long residence time
78 of about 40 years in the SCS (Feng et al., 1999; Li et al., 2018; Su and Yuan, 2005).
79 The distributions of phytoplankton and primary productivity of the SCS show great
80 temporal and spatial variation (Ning et al., 2004). Low chlorophyll a (Chl a) and
81 primary production are the significant characteristics of the SCS basin which is
82 considered an oligotrophic region, and macronutrients (i.e. nitrogen) are the main
83 limitations of phytoplankton growth and productivity (Ning et al., 2004; Lee Chen,
84 2005; Han et al., 2013). The excessive runoff from Pearl River can result in high N/P
85 (nitrogen/phosphorus) ratio of > 100 , shifting the nutritive state from nitrogen
86 deficiency to phosphorus deficiency in the coastal region of SCS (Lee Chen and Chen,
87 2006). Dissolved iron is also a potential limitation on primary production, especially in
88 the high nutrient low chlorophyll (HNLC) regions (Cassar et al., 2011). But on the
89 northern slope of the SCS, the concentration of dissolved iron is high enough to support

90 the growth of phytoplankton in the surface water (Zhang et al., 2019). The northern
91 slope of the SCS is an important transition region between coastal area and the SCS
92 basin. In the summer, the shelf water intrusion is an important process changing the
93 nutritive state in the northern slope region of the SCS (He et al., 2016; Lee Chen and
94 Chen, 2006). But so far, the NCP enhancement caused by this process is still unknown.

95 Previous studies about the organic carbon export in the SCS were mostly conducted
96 on particulate organic carbon (POC) flux (e.g., Bi et al., 2013; Cai et al., 2015; Chen et
97 al., 1998; Chen et al., 2008; Ma et al., 2008; Ma et al., 2011). Little research has been
98 conducted on NCP in the SCS to date. Chou et al. (2006) estimated NCP in the northern
99 SCS during the summertime to be $4.47 \text{ mmol C m}^{-2} \text{ d}^{-1}$ based on the time change rate
100 of dissolved inorganic carbon (DIC) in the mixed layer at the South East Asia Time-
101 Series Station (SEATS) from 2002 to 2004. Wang et al. (2014) used GPP and CR data
102 from a light/dark bottle incubation experiment to calculate NCP in the northern SCS
103 and obtained a range from -179.0 to $377.6 \text{ mmol O}_2 \text{ m}^{-2} \text{ d}^{-1}$ (-129.7 to 273.6 mmol C
104 $\text{m}^{-2} \text{ d}^{-1}$). Huang et al. (2018) estimated monthly NCP from July 2014 to July 2015 based
105 on in situ O_2 measurements on an Argo profiling float and reported the cumulative NCP
106 to be $0.29 \text{ mol C m}^{-2} \text{ month}^{-1}$ ($9.67 \text{ mmol C m}^{-2} \text{ d}^{-1}$) during the northeast monsoon
107 period and $0.17 \text{ mol C m}^{-2} \text{ month}^{-1}$ ($5.67 \text{ mmol C m}^{-2} \text{ d}^{-1}$) during the southwest
108 monsoon period in the SCS basin. However, most of these studies in the SCS were
109 constrained by methodological factors attributed to discrete sampling and cannot reveal
110 the rapid productivity response to highly dynamic environmental fluctuations of coastal
111 systems. Discrete sampling suffers from low spatial resolution, and cannot adequately
112 resolve variabilities caused by small-scale physical or biological processes in the
113 dynamic marine systems. In addition, each of the three methods for NCP estimate
114 mentioned above has its limitation. DIC-based NCP estimate is not suitable for the
115 coastal region, because instead of biological metabolism, the terrestrial runoff can be
116 the strongest factor influencing the DIC in the coastal system (Mathis et al., 2011). The
117 unavoidable difference between in situ circumstance and on-deck incubation condition
118 can introduce uncertainties to the NCP derived from light/dark bottle incubation
119 (Grande et al., 1989). Though Argo profiling float partly gets rid of the limitation of

120 discrete sampling, it's hard to control its movement in the study region. However, no
121 high-resolution measurement of NCP has been reported for the SCS so far.

122 In this paper, we present high-resolution NCP estimates in the northern slope region
123 of the SCS based on continuous shipboard dissolved O₂/Ar measurement. We discuss
124 the regulating factors of NCP based on ancillary measurements of other hydrographic
125 parameters. Our high-resolution measurements caught the rapid response of the
126 ecosystem to the episodic nutrient supply induced by eddies and help us to quantify the
127 contribution of eddy-entrained shelf water intrusion to NCP in the summer cruise.

128

129 **2. Methods**

130 **2.1 Continuous underway sampling and measurement**

131 Continuous measurements of dissolved gases (O₂, Ar, and CO₂) were obtained using
132 membrane inlet mass spectrometry (MIMS, HPR 40, Hiden Analytical, UK) (Tortell,
133 2005) onboard the *RV 'Nanfeng'* during two cruises in the northern slope region of the
134 SCS (Figures 1a, 1b) from 13 to 23 October 2014 and from 13 to 29 June 2015. In
135 addition, a cyclonic-anticyclonic eddy pair was observed in June 2015 (Figure 1c) and
136 resulted in dramatic influences on the study region.

137 We developed a continuous shipboard measurement system of dissolved gases
138 following the method described by Guéguen and Tortell (2008). Surface seawater was
139 collected continuously using the ship's underway intake system (~5 m depth) and was
140 divided into different lines for various underway scientific measurements. Seawater
141 from the first line passed through a chamber at a flowrate of 2–3 L min⁻¹ to remove
142 macroscopic bubbles and to avoid pressure bursts. A flow of ~220 mL min⁻¹ was
143 continuously pumped from the chamber using a Masterflex Peristaltic Pump equipped
144 with L/S® multichannel cartridge pump heads (Cole Parmer). In order to minimize the
145 O₂/Ar fluctuations due to temperature effects and water vapor pressure variations, the
146 water samples flowed through a stainless steel coil (~6 m) with 0.6 mm wall thickness
147 immersed in a water bath (Shanghai Bilon Instrument Co. Ltd, China) to achieve a
148 constant temperature (~2 °C below the sea surface temperature), which avoided

149 temperature-induced supersaturation and subsequent bubble formation. Then the water
150 samples were introduced into a cuvette with a silicone membrane mounted on the inside.
151 The analyte gases were monitored by a Faraday cup detector in the vacuum chamber
152 after diffusion through the silicone membrane, and the signal intensities at the relevant
153 mass to charge (m/z) ratios (32, 40 and 44 for O_2 , Ar and CO_2 , respectively) were
154 recorded by MASsoft. Based on the continuous measurement of 50 L air-equilibrated
155 seawater, the long-term signal stability (measured as the coefficient of variation) over
156 12 h was 1.57 %, 3.75 % and 2.21 % for O_2 , Ar and CO_2 , respectively. Seawater from
157 the second line passed through a flow chamber, where an RBR Maestro (RBR, Canada)
158 was installed to continuously record temperature, salinity, dissolved oxygen (DO), and
159 Chl a. We didn't obtain continuous DO data in October 2014 because the DO sensor of
160 RBR broke down. A third line was used to drain the excess seawater. Underway
161 pipelines were flushed with freshwater or bleach every day, to avoid possible in-lines
162 biofouling. The data from the underway transects were exported to spreadsheets and
163 compiled into 5 min averages, and the comparisons of the gas data with other
164 hydrographic variables were based on the UTC time recorded for each measurement.

165 The O_2/Ar ratio measurements were calibrated with air-equilibrated seawater samples
166 at about 6–8 h intervals to monitor instrument drift and calculate $\Delta(O_2/Ar)$. These air-
167 equilibrated seawater samples were prefiltered (0.22 μm) and bubbled with ambient air
168 for at least 24 h to reach equilibrium at sea surface temperature (Guéguen and Tortell,
169 2008). For calibration, 800 mL of air-equilibrated seawater sample was transferred into
170 glass bottles and immediately drawn into the cuvette, where the first 200 mL of the
171 sample was used to flush the cuvette and pipelines. After 3 min recirculation of the
172 sample, the average signal intensity was obtained to calculate O_2/Ar . During the course
173 of measurements, flow rate and the temperature of water bath were both kept the same
174 as the underway measurements. The precision of MIMS-measured O_2/Ar was 0.22 %,
175 based on analyses of 20 duplicate samples in the laboratory test, which is comparable
176 to previous studies and sufficient to detect biologically driven gas fluctuations in
177 seawater (Tortell, 2005).

178 The instrumental CO_2 ion current was calibrated at about 12–24 h intervals using

179 equilibrated seawater standards as per Guéguen and Tortell (2008) during the survey in
 180 June 2015. Prefiltered seawater (0.22 μm) was gently bubbled with dry CO_2 standards
 181 (200, 400, and 800 ppm, provided by the Chinese National Institute of Metrology) at in
 182 situ temperature. After 2 days of equilibrium, these standards were analyzed by MIMS
 183 following the same procedure for measuring air-equilibrated seawater samples to obtain
 184 a calibration curve between CO_2 signal intensity and mole fraction. The reproducibility
 185 of these measurements was better than 5 % within 15 days. Then we used the empirical
 186 equations reported by Takahashi et al. (2009) to convert the CO_2 mole fraction derived
 187 from the calibration curve to the in situ partial pressure of CO_2 ($p\text{CO}_2$).

188 Chlorophyll-a (Chl a) data from the RBR sensor were linear calibrated against
 189 extracted Chl a measurements of discrete seawater samples taken from the same
 190 seawater outlet as for MIMS measurements. Samples were filtered through
 191 polycarbonate filters (0.22 μm). The filter membranes were then packed with pre-
 192 sterilized aluminum foil and stored in a freezer ($-20\text{ }^\circ\text{C}$) until extraction by acetone and
 193 analysis using a fluorimetric method (F-4500, HITACHI, Japan) described by Parsons
 194 (1984). The mean residual of this calibration was $0.00 \pm 0.07\ \mu\text{g L}^{-1}$.

195

196 **2.2 Estimation of NCP based on O_2/Ar measurements**

197 NCP in the mixed layer was estimated by the O_2/Ar mass balance from continuous
 198 measurements. Due to similar physical properties of O_2 and Ar, $\Delta(\text{O}_2/\text{Ar})$ is used as a
 199 proxy of the biological O_2 supersaturation and is defined as (Craig and Hayward, 1987):

$$200 \quad \Delta(\text{O}_2 / \text{Ar}) = \frac{([\text{O}_2]/[\text{Ar}])}{([\text{O}_2]/[\text{Ar}]_{\text{eq}})} - 1$$

201 where $[\text{O}_2]/[\text{Ar}]$ is the measured dissolved O_2/Ar ratio of the mixed layer and
 202 $([\text{O}_2]/[\text{Ar}]_{\text{eq}})$ is the measured dissolved O_2/Ar ratio of the air-equilibrated seawater
 203 samples. $\Delta(\text{O}_2/\text{Ar})$ is the percent deviation of the measured O_2/Ar ratio from the
 204 equilibrium. Assuming a steady state and negligible physical supply, NCP is the air-
 205 sea biological O_2 flux and can be estimated as (Reuer et al., 2007):

$$206 \quad \text{NCP} \text{ (mmol C m}^{-2} \text{ d}^{-1}) \approx k_{\text{O}_2} \cdot [\text{O}_2]_{\text{sat}} \cdot \Delta(\text{O}_2 / \text{Ar}) \cdot r_{\text{C:O}_2} \cdot \rho$$

207 where k_{O_2} is the weighted gas transfer velocity of O_2 (m d^{-1}); $[\text{O}_2]_{\text{sat}}$ denotes the

208 saturation concentration of dissolved O_2 ($\mu\text{mol kg}^{-1}$) in the mixed layer, which is
209 calculated based on temperature and salinity (Weiss, 1970); $r_{C:O_2}$ is the photosynthetic
210 quotient of C and O_2 and was reported as 1:1.38 in the SCS (Jiang et al., 2011); ρ is
211 seawater density in units of kg m^{-3} (Millero and Poisson, 1981). We estimated k_{O_2}
212 using the European Centre for Medium-Range Weather Forecasts (ECWMF) wind-
213 speed reanalysis data product with a $0.25^\circ \times 0.25^\circ$ grid (<https://www.ecmwf.int>), the
214 parameterization by Wanninkhof (1992), and the gas exchange weighting algorithm by
215 Teeter et al. (2018). Teeter et al., (2018) pointed out that modern O_2/Ar method does
216 not strongly rely on the steady state assumption. When this assumption is violated, our
217 estimate does not represent the actual daily NCP but rather an estimate of NCP
218 weighted over the residence time of O_2 in the mixed layer and along the path of the
219 water parcel during that period. Thus the residence time of O_2 in the mixed layer is an
220 important implication of the weighted timescale of NCP before the measurement of
221 O_2/Ar . The residence time of O_2 (τ , d) in the mixed layer is estimated as the ratio of
222 mixed layer depth (MLD, m) to the gas transfer velocity of O_2 (k_{O_2} , m d^{-1}) (Jonsson
223 et al., 2013).

224

225 **2.3 Ancillary measurements and calculations**

226 Surface water samples for the nutrient analysis were collected from Niskin bottles
227 mounted on the CTD, where the samples were filtered through acid-cleaned acetate
228 cellulose filters (pore size: $0.4 \mu\text{m}$). The filtrates were poisoned by HgCl_2 and stored in
229 the dark at 4°C . In the laboratory, the nutrients were determined photometrically by an
230 auto-analyzer (QuAatro, SEAL Analytical, Germany) with a precision better than 3 %.
231 MLD was defined by the $\Delta\sigma_t = 0.125 \text{ kg m}^{-3}$ criterion (Monterey and Levitus, 1997).
232 The subsurface chlorophyll maximum layer (SCML) was observed using the
233 fluorescence sensor mounted on the CTD. SCML usually occurs at the bottom of
234 euphotic layer (Hanson et al., 2007; Liao et al., 2018; Teira et al., 2005). Because no
235 PAR (Photosynthetically Available Radiation) profile data were obtained in two cruises,
236 we decided to regard the depth of SCML as the euphotic depth (Z_{eu}). Both MLD and
237 Z_{eu} were calculated at each station where the vertical CTD casts were made. The MLDs

238 for underway data between CTD stations was calculated using linear interpolation
239 based on the distance between the underway points and nearest CTD stations. We
240 matched the underway data to each CTD location using a combination of
241 latitude/longitude threshold (latitude/longitude of CTD station $\pm 0.05^\circ$) and time
242 threshold (end/start of stationary time ± 1 h), then took the averages of these underway
243 data for further analysis with discrete nutrient concentrations.

244 The daily satellite chlorophyll data were obtained from the E.U. Copernicus Marine
245 Service Information website (<https://resources.marine.copernicus.eu>). The product we
246 used was provided by ACRI-ST company (Sophia Antipolis, France), with a space-
247 time interpolation (the “Cloud Free”). The M_Map package for Matlab was applied to
248 output satellite chlorophyll images (Pawlowicz, 2020). Daily and 8-day PAR data
249 collected by MODIS-Aqua sensor were obtained from NASA’s ocean color website
250 (<https://oceancolor.gsfc.nasa.gov/l3>). The spatial resolution of both satellite products is
251 4 km, and we match the satellite PAR with CTD location by choosing the closest PAR
252 data point to the CTD location. A light attenuation coefficient (K_d , m^{-1}) was used to
253 estimate the average PAR in the mixed layer (Kirk 1994; Jerlov 1976):

254
$$K_d = \frac{4.605}{Z_{eu}}$$

255 **3. Results and Discussion**

256 **3.1 Distributions of hydrographic parameters and gases**

257 The distributions of temperature, salinity, Chl a, and $\Delta(O_2/Ar)$ during the autumn cruise
258 (October 2014) are shown in Figure 2. Sea surface temperature (SST) ranged from
259 26.96 °C to 28.53 °C with an average of 27.82 ± 0.33 °C. Sea surface salinity (SSS)
260 ranged from 33.28 to 34.11 with the low values occurring in the southeast of the region.
261 Chl a concentration ranged from 0.01 to 0.71 $\mu g L^{-1}$ and was in an average of $0.18 \pm$
262 $0.13 \mu g L^{-1}$, which was comparable to the 11-year mean value ($\sim 0.2 mg m^{-3}$) in the
263 same region in October reported by Liu et al. (2014). $\Delta(O_2/Ar)$ values were in the range
264 of $-2.9-4.9$ % (avg. 1.1 % ± 0.9 %) and slightly oversaturated in most areas (Figure
265 2d). Please note that all averages we have published in this paper are reported in the

266 format of *mean* \pm *standard deviation*.

267 In June 2015, SST ranged from 29.28 °C to 32.24 °C and was in an average of 30.88
268 \pm 0.59 °C (Figure 3a). SSS ranged from 30.81 to 34.16. Transect 3 was significantly
269 characterized by low salinity (Figure 3b). He et al (2016) reported that this phenomenon
270 was influenced by the eddy-entrained Pearl River plume (shelf water) injected into the
271 SCS. Chl a varied in a range of 0.09–0.58 $\mu\text{g L}^{-1}$ in the study region. Under the influence
272 of this eddy-entrained shelf water, Chl a values higher than 0.30 $\mu\text{g L}^{-1}$ were observed
273 along Transect 3 (Figure 3c). In contrast, Chl a was in the range of 0.09–0.18 $\mu\text{g L}^{-1}$
274 along Transect 1 and 2. It was obvious that DO was much higher in the east side than
275 the west side in the study region (Figure 3d). $\Delta(\text{O}_2/\text{Ar})$ ranged from -3.9 – 13.6 %. Most
276 of the $\Delta(\text{O}_2/\text{Ar})$ values were positive in the study region (avg. 2.7 % \pm 2.8 %), whereas
277 the negative values were concentrated along Transect 4 (Figure 3f). $\Delta(\text{O}_2/\text{Ar})$ along
278 Transect 3 was in an average of 7.2 % \pm 2.6 %, significantly higher than that of other
279 transects (Figure 3f). $p\text{CO}_2$ exhibited a high degree of spatial and temporal variability
280 and the high values mostly occurred on the west side of the study region (Figure 3e).
281 Resulting from the considerable low $p\text{CO}_2$ in Transect 3, the average $p\text{CO}_2$ (323 ± 93
282 μatm) in the study region was lower than those reported previously, i.e., 350–370 μatm
283 by Zhai et al (2009) and 340–350 μatm by Rehder and Sues (2001). Due to the influence
284 of the shelf water, the average $p\text{CO}_2$ in Transect 3 was 222 ± 33 μatm , with a range of
285 144–321 μatm . In the summer, shelf water mixed with Pearl River plume is the most
286 important factor influencing $p\text{CO}_2$ in the coastal and shelf region of the northern SCS,
287 which can result in the $p\text{CO}_2$ values as low as 150 μatm (Li et al., 2020). Here we apply
288 an average atmospheric $p\text{CO}_2$ of 382 μatm that observed in July 2015 in the northern
289 SCS (Li et al., 2020) to calculate the $p\text{CO}_2$ difference ($\Delta p\text{CO}_2$) between the surface
290 water and the atmosphere. $\Delta p\text{CO}_2$ ranged from -238 to -61 μatm along Transect 3,
291 indicative of a strong CO_2 sink.

292

293 **3.2 Mixed layer depth, euphotic depth and residence time of O_2 in the mixed layer**

294 MLD, euphotic depth (Z_{eu}) and the residence time of O_2 (τ) in the mixed layer at CTD
295 stations of two cruises are shown in Table 1 and 2. In autumn 2014, MLD ranged from

296 27 to 81 m, with an average of 55 ± 15 m (Table 1). The average Z_{eu} was 74 ± 12 m,
297 approximately 20 m deeper than MLD (Table 1). The residence time of O_2 in the mixed
298 layer ranged from 3 to 13 d (Table 1), comparable to a range of 1–2 weeks reported by
299 previous studies (Izett et al., 2018; Manning et al., 2017). The average residence time
300 of O_2 was 9 ± 3 d, indicating that our estimate generally quantified NCP over 9 days
301 prior to the underway observation of O_2/Ar during this cruise.

302 The average MLD in June 2015 was just 18 ± 6 m (Table 2). Significant shallow MLD
303 occurred at two stations (J-10, J-11) located in Transect 3 (Table 2, Figure S1f). The
304 low-salinity shelf water intrusion is the main cause of this shallow MLD of 8 m. The
305 average Z_{eu} was 58 ± 18 m, approximately 40 m deeper than MLD (Table 2). The
306 residence time of O_2 in the mixed layer ranged from 2 to 12 d (Table 2), indicating a
307 fast gas exchange in some stations. In addition, we also observed relatively obvious
308 subsurface O_2 maxima in Transect 1 and 2 in summer 2015. But this phenomenon didn't
309 exist in autumn 2014.

310 In both cruises, Z_{eu} was observed obviously deeper than MLD. This result partly
311 suggests that light availability may not be a limitation of NCP in the northern slope of
312 SCS. Especially in the summer, Z_{eu} extended to 2–7 times of MLD (Table 2), ensuring
313 sufficient illumination in the mixed layer. But in the autumn when the thickness of
314 mixed layer accounts for about 74 % of euphotic layer, the average light intensity in the
315 mixed layer might be influenced by the exponentially light attenuation along depth.

316

317 **3.3 NCP in autumn and summer**

318 In October 2014, NCP in the northern slope of the SCS ranged from -29.2 to 42.7 mmol
319 $C\ m^{-2}\ d^{-1}$ (avg. 11.5 ± 8.7 mmol $C\ m^{-2}\ d^{-1}$) and most of the region was net autotrophic
320 (Figure 4a). The estimated NCP based on the O_2/Ar values measured in this cruise is
321 about 34 % of the net primary production rates of 34.3 mmol $C\ m^{-2}\ d^{-1}$ measured by
322 ^{14}C bottle incubation (Sun X., personal communication), which was in agreement with
323 previous research (Quay et al., 2010).

324 The average NCP in the study region was 11.6 ± 12.7 mmol $C\ m^{-2}\ d^{-1}$ with a range of
325 -27.6 – 61.4 mmol $C\ m^{-2}\ d^{-1}$ in June 2015. A high NCP level was observed along

326 Transect 3 (Figure 4b). Eddy-entrained shelf water brought a large amount of
327 terrigenous nutrients from the shelf to the slope region along Transect 3 (He et al., 2016).
328 The average nitrate (NO_3^-) and nitrite (NO_2^-) concentrations in the surface water of
329 Transect 3 were $2.31 \pm 0.70 \mu\text{mol L}^{-1}$ and $0.04 \pm 0.01 \mu\text{mol L}^{-1}$ respectively (Figure
330 S1a, S1b); both values were much higher than those found in the other three transects
331 where NO_3^- was in a range of $< 0.03\text{--}0.69 \mu\text{mol L}^{-1}$ and NO_2^- was mostly below the
332 detection limit. Li et al. (2018) reported that the entire Transect 3 and part of Transect
333 4 were dominated by shelf water at the surface and we estimated NCP over these regions
334 where salinity lower than 33 as $23.8 \pm 10.7 \text{ mmol C m}^{-2} \text{ d}^{-1}$ on average. We also
335 observed a warm eddy (anti-cyclone) covering most stations in Transects 1 and 2
336 (Figure 1b, 1c) during our survey in June 2015 (Chen et al., 2016). Anti-cyclonic eddies
337 can cause downwelling, deepening of the thermocline, and blocking of the supply of
338 nutrients from the deeper water (Ning et al., 2008; Shi et al., 2014). Consequently, a
339 warm eddy is expected to result in an oligotrophic condition in the surface water
340 associated with low Chl a concentrations and low production (Ning et al., 2004). As a
341 result, in the summer of 2015, the observed NO_2^- , NO_3^- , and PO_4^{3-} (phosphate)
342 concentrations were almost below the detection limit in Transects 1 and 2 (Figure S1a,
343 S1b, S1d). NCP in Transect 1 and 2 was at a very low level (avg. $2.8 \pm 2.7 \text{ mmol C m}^{-2}$
344 d^{-1}). Because of the significant high values of NCP over the regions with shelf water
345 intrusion, our NCP result in the summer of 2015 is averagely higher than the previous
346 values of $4.47 \text{ mmol C m}^{-2} \text{ d}^{-1}$ and $0.17 \text{ mol C m}^{-2} \text{ month}^{-1}$ ($5.67 \text{ mmol C m}^{-2} \text{ d}^{-1}$)
347 based on DIC budget and Argo- O_2 respectively in the SCS (Chou et al., 2006; Huang
348 et al., 2018). However, NCP estimates based on both methods mentioned above suffer
349 from poor temporal and spatial coverage and do not allow for revealing rapid changes
350 in shelf systems. In contrast, continuous measurements of O_2/Ar allow us to capture
351 rapid variations in NCP along Transect 3 and resolve short-term productivity responses
352 to environmental fluctuations.

353

354 **3.4 Distribution of various parameters along representative transects**

355 We chose Transect 5 (Figure 1a) observed in October 2014 and Transect 4 (Figure 1b)

356 observed in June 2015 to show the distribution of various parameters.

357 The distribution of Chl a, $\Delta(\text{O}_2/\text{Ar})$, and NCP showed similar trend along Transect 5
358 in October 2014 (Figure 5). There was a trough of temperature, showing a maximum
359 drawdown of ~ 0.6 °C compared to the average temperature in the study region (Figure
360 5a). But the temperature fluctuations shown here are too small to reflect a significant
361 upwelling that can easily cause ~ 2 °C drawdown of temperature in the upper layer (Lin
362 et al., 2013; Manning et al., 2017; Ning et al., 2004). A spike of Chl a occurred between
363 115.6°E and 115.7°E and was coincident with the peaks of $\Delta(\text{O}_2/\text{Ar})$ and NCP (Figure
364 5b, 5c). The highest surface concentration of ammonium (NH_4^+) of $0.35 \mu\text{mol L}^{-1}$ was
365 also observed between 115.6°E and 115.7°E in this transect and was predominantly
366 higher than the concentrations ($0.07\text{--}0.17 \mu\text{mol L}^{-1}$) in the other regions of this cruise
367 (Figure 5c, S2b). Because no significant obduction processes (i.e., upwelling,
368 entrainment, and diapycnal mixing) were reported in this region, the most likely source
369 of this abundant NH_4^+ was in situ regeneration such as the excretion of zooplankton and
370 the bacterial decomposition of organic matter (La Roche, 1983; Clark et al., 2008).
371 Theoretically, NH_4^+ , an important nitrogen source of phytoplankton growth, can be
372 quickly utilized by phytoplankton, and contributes to primary production (Dugdale and
373 Goering, 1967; Tamminen, 1982). However, we only got nutrient data at two CTD
374 stations in this transect, thus the result we obtained here just indicated that high NCP
375 occurred at the station with relatively high NH_4^+ concentration, but couldn't be a strong
376 evidence that NH_4^+ was the main factor influencing NCP in this transect.

377 A similar distribution pattern of Chl a, NCP, and $\Delta(\text{O}_2/\text{Ar})$ was observed along
378 Transect 4 in June 2015, whereas $p\text{CO}_2$ showed the opposite trend for these three
379 parameters (Figure 6b, 6c). Low salinity (lower than 33) existed at both southern and
380 northern ends of this transect (Figure 6a). The concentration of dissolved inorganic
381 nitrogen (DIN , $\text{NO}_3^- + \text{NO}_2^- + \text{NH}_4^+$) in the surface water was $0.81 \mu\text{mol L}^{-1}$ and 0.27
382 $\mu\text{mol L}^{-1}$ at the southern and northern end respectively, which was higher than the
383 concentrations in other stations of this transect (Figure 6c). These results indicate that
384 shelf water is imported at the northern and southern ends of this transect, along with
385 higher levels of Chl a and NCP (Figure 6c). A sharp drop in the temperature and an

386 increase in salinity occurred from 19.7°N to 19.8°N and from 21°N to 20.7°N (Figure
387 6a), manifesting an upwelling over this area together with dramatic spikes in $p\text{CO}_2$ and
388 associated decrease in $\Delta(\text{O}_2/\text{Ar})$ (Nemcek et al., 2008) (Figure 6b). Most regions of
389 Transect 4 were dominated by upwelling and showed negative sea level height anomaly
390 (Chen et al., 2016; He et al., 2016). A localized cold eddy was considered the cause of
391 this upwelling (Figure 1c), resulting in a maximum temperature drawdown of ~ 1.6 °C
392 in the mixed layer.

393 Vertical mixing is considered the largest source of error in O_2/Ar -based NCP estimates
394 because the upwelled subsurface water with different O_2/Ar signatures can produce
395 either an overestimation or an underestimation of NCP in the mixed layer (Cassar et al.,
396 2014; Izett et al., 2018). Former researches usually ignored the underestimated negative
397 NCP that caused by vertical mixing (Giesbrecht et al., 2012; Reuer et al., 2007; Stanley
398 et al., 2010). Cassar et al. (2014) presented a N_2O -based correction method of O_2/Ar
399 and NCP for vertical mixing. Although this method has been successfully adopted by
400 Izett et al. (2018) in the Subarctic Northeast Pacific, it is not suitable for our study
401 region. This is because it is basically applicable in the areas where the depths of
402 euphotic zone and mixed layer are similar, and this method is not suitable for
403 oligotrophic regions (Cassar et al., 2014). The SCS is recognized as an oligotrophic
404 region and the depth of the euphotic zone can be 2–7 times that of the mixed layer in
405 our study region in the summer. In addition, in the region (e.g. the SCS basin) where
406 subsurface oxygen maximum exists, the applicability of N_2O -based correction method
407 is limited (Izett et al., 2018). In Transect 4, the regions with negative NCP and the
408 regions with salinity higher than 33.5 and temperature lower than 30 °C are defined as
409 influenced by upwelling. If we neglect these regions in Transect 4, the average NCP in
410 June 2015 can slightly raise to 12.4 ± 12.3 mmol C $\text{m}^{-2} \text{d}^{-1}$. If we also remove the
411 influence of shelf water intrusion by neglecting the regions with salinity lower than 33,
412 the average NCP can sharply decrease to 5.0 ± 6.2 mmol C $\text{m}^{-2} \text{d}^{-1}$, which was similar
413 to the results of 4.47 mmol C $\text{m}^{-2} \text{d}^{-1}$ and 0.17 mol C $\text{m}^{-2} \text{month}^{-1}$ (5.67 mmol C m^{-2}
414 d^{-1}) reported in previous researches in the same season (Chou et al., 2006; Huang et al.,
415 2018). Here we regard 5.0 ± 6.2 mmol C $\text{m}^{-2} \text{d}^{-1}$ as the background value of NCP in the

416 study region. Since an average NCP of $23.8 \pm 10.7 \text{ mmol C m}^{-2} \text{ d}^{-1}$ was observed over
417 the regions with salinity lower than 33, we can conclude that the summer shelf water
418 intrusion significantly promoted NCP by potentially more than threefold in June 2015.

419

420 **3.5 Factors influencing NCP in the SCS**

421 The SCS is an oligotrophic region with low biomass and primary production (Lee Chen,
422 2005; Ning et al., 2004). Previous research has shown that the nutrient, especially
423 nitrogen and phosphorus, is the most important factor controlling and limiting the
424 phytoplankton biomass and primary production in the SCS (Ning et al., 2004; Lee Chen,
425 2005; Lee Chen and Chen, 2006; Han et al., 2013). After neglecting the two CTD
426 stations (J-14, J-15) with negative NCP influenced by upwelling in June 2015, we
427 performed a principal component analysis (PCA) to determine the dominant factors
428 influencing NCP in both cruises. In October 2014, DIN (0.741), $\Delta(\text{O}_2/\text{Ar})$ (0.858), and
429 NCP (0.979) were significantly loaded on Factor 1, indicating a potential relationship
430 among these three variables (Figure 7a, Table S1b). The correlation coefficient between
431 DIN and NCP was 0.706 ($p < 0.01$, Table S1a), which was significantly higher than the
432 coefficient between NCP and the other variables, except for $\Delta(\text{O}_2/\text{Ar})$ and temperature;
433 this indicated that DIN was an important factor influencing NCP in this cruise. Another
434 two nutrients – dissolved silicate (DSi, SiO_3^{2-}) and dissolved inorganic phosphorus
435 (DIP, PO_4^{3-}) – had no correlations ($p > 0.05$) with NCP (Table S1a). In June 2015,
436 Factor 1 showed a strong loading by DIN (0.876), Chl a (0.950), DO (0.927), $\Delta(\text{O}_2/\text{Ar})$
437 (0.902), and NCP (0.909), whereas salinity (-0.936) and $p\text{CO}_2$ (-0.908) were
438 negatively loaded on Factor 1 (Figure 7b, Table S2b). The injection of low salinity shelf
439 water appeared to have a strong effect on the study region because significant negative
440 correlations were observed between salinity and DIN, Chl a, $\Delta(\text{O}_2/\text{Ar})$, and NCP (Table
441 S2a). DIN had strong correlations with NCP, $\Delta(\text{O}_2/\text{Ar})$, and Chl a, with the correlation
442 coefficients of 0.747, 0.910, and 0.754, respectively (Table S2a), indicating that DIN
443 was the dominant factor controlling the growth of phytoplankton and primary
444 production in this cruise. DSi (0.582) and DIP (-0.601) were both moderately loaded
445 on Factor 2 (Figure 7b, Table S2b) and had no correlations with NCP ($p > 0.05$, Table

446 S2a). These results suggested the key role of nitrogen in regulating $\Delta(\text{O}_2/\text{Ar})$, NCP, and
447 phytoplankton biomass in the SCS. The supply of nitrogen may stimulate the growth of
448 phytoplankton in the SCS and nitrogen is an important participant in photosynthesis
449 and a basic element that contributes to the increase in primary production (Dugdale and
450 Goering, 1967; Lee Chen, 2005; Lee Chen and Chen, 2006; Han et al., 2013).

451 Coupled with biochemical variations, physical processes also play important roles in
452 the slope region of the SCS by transporting abundant nutrient-rich shelf water into the
453 SCS and bringing deep water to the surface by enhancing water mixing (Chen and Tang,
454 2012; Ning et al., 2004; Pan et al., 2012). The surface waters in the slope region of the
455 northern SCS are primarily composed of waters originating from SCS water, Kuroshio
456 water, and shelf water (Li et al., 2018). In the summer, the shelf water exists where the
457 potential density anomaly is lower than 20.5 kg m^{-3} (Li et al., 2018). In the autumn,
458 there is a weak offshore transport of the shelf water in the SCS and the salinity of the
459 water mixed with the shelf water is usually lower than 33 (Fan et al., 1988; Uu and
460 Brankart, 1997; Su and Yuan, 2005). In October 2014, the observed surface salinity was
461 in a range of 33.28 to 34.11; thus the surface waters were mainly derived from mixing
462 of the Kuroshio water and the SCS water. In the summer of 2015, a cyclonic-
463 anticyclonic eddy pair was observed in the study region (Figure 1c). Low-salinity shelf
464 water mixed with the intruding river plume from the Pearl River in the upper 50 m and
465 was transported to the slope and basin along the intersection of the two eddies (Chen et
466 al., 2016; He et al., 2016; Li et al., 2018). In both seasons, the surface waters in the
467 study region were generally found to be nitrogen deficient, with NO_2^- at $< 0.01\text{--}0.04$
468 $\mu\text{mol L}^{-1}$ (Figure S2a, S1b), NO_3^- at $< 0.03\text{--}2.82 \mu\text{mol L}^{-1}$ (Figure S1a), and NH_4^+ at
469 $0.04\text{--}0.35 \mu\text{mol L}^{-1}$ (Figure S2b, S1c). The concentrations of NO_2^- and NO_3^- were
470 below the detection limit at almost 80% of the sampling stations during both cruises.
471 Due to the injection of shelf water with low salinity and abundant terrestrial nutrients,
472 significant high concentrations of NO_3^- and NO_2^- were observed along Transect 3 in
473 June 2015 (Figure S1a, S1b) where the shelf water was intruded by eddies (Chen et al.,
474 2016; He et al., 2016). Such transport processes from the inner shelf to the slope region
475 have a profound influence on nutrient dynamics and biological productions (He et al.,

476 2016). The water that was influenced by shelf water with a potential density anomaly
477 lower than 20.25 kg m^{-3} and salinity lower than 33 had high concentrations of DIN
478 (Figure 8a). At the 6 stations (in the red circle of Figure 8a) that were intruded by shelf
479 water and characterized with surface salinity lower than 33, we obtained an average
480 surface DIN concentration of 1.82 ± 1.16 ($0.27\text{--}3.01$) $\mu\text{mol L}^{-1}$, which was significantly
481 higher than the mean of 0.10 ± 0.03 ($0.04\text{--}0.16$) $\mu\text{mol L}^{-1}$ at other stations (independent
482 samples t-test, $p < 0.01$). After neglecting the two stations (J-14, J-15) influenced by
483 upwelling, a strong correlation between NCP and DIN was observed in the cruise of
484 June 2015 ($r = 0.747$, $p < 0.01$), with higher NCP (avg. $15.4 \pm 4.5 \text{ mmol C m}^{-2} \text{ d}^{-1}$)
485 occurred at the stations where shelf water intruded, consistent with the DIN
486 concentration higher than $0.27 \mu\text{mol L}^{-1}$ (Figure 8b). At other stations without the
487 influence of shelf water, the average NCP was just $2.3 \pm 1.7 \text{ mmol C m}^{-2} \text{ d}^{-1}$. These
488 results furtherly suggest that the supply of DIN from shelf water can greatly stimulate
489 the primary production at these stations, resulting in the NCP increase of nearly 7 times
490 compared to other stations.

491 The correlations between NCP and sea surface temperature and salinity also support
492 the influence of physical forcing on NCP. In June 2015, we obtained a strong negative
493 correlation between NCP and salinity (Figure 9d). NCP significantly increased in the
494 water with salinity lower than 33 (Figure 9d). Temperature had weak correlations with
495 NCP (Figure 9c), and the negative NCP values were concentrated in the water with
496 temperatures below $30.5 \text{ }^\circ\text{C}$ and salinity values over 33.5 (Figure 9c, 9d). This surface
497 water was mostly observed along Transect 4 where vertical mixing caused by a cold
498 eddy brought deep water to the surface. The undersaturated $\Delta(\text{O}_2/\text{Ar})$ entrained by deep
499 water caused the negative NCP estimates at the surface, resulting in a considerable
500 underestimation of NCP. Unlike in June 2015, all the correlations were very weak
501 between NCP and temperature, salinity in October 2014 (Figure 9a, 9b). The Kuroshio
502 water and the SCS water had similar hydrological characteristics and their mixing in
503 October 2014 may not have resulted in significant changes in the hydrological
504 characteristics of the surface water.

505 The nutrient concentrations and hydrographic characteristics we observed just reflect

506 the marine environment at the moment of sampling, partly contradicting our estimates
507 that quantified NCP over a period prior to the observation. Especially for the regions
508 with significant influence of shelf water in June 2015, tracking the history of shelf water
509 intrusion is important. We used daily satellite chlorophyll data to monitor the intrusion
510 of shelf water and roughly set satellite-chlorophyll $\geq \sim 0.2 \mu\text{g L}^{-1}$ as the criterion of
511 shelf water (Figure 10). On 10 June 2015, shelf water began to influence the northern
512 end (J-9) of Transect 3 and most part of Transect 4, then it extended to the southern end
513 of Transect 3 and Transect 4 where J-12 and J-13 located on 13 June (Figure 1b, 10).
514 Till 25 June when we finished the observation of Transect 4, the entire Transect 3 (J-9
515 to 12) as well as J-13 and J-16 had kept been dominated by shelf water for more than
516 10 days (Figure 1b, 10). We concluded these findings in Table 3, along with the
517 residence time (τ) of O_2 in the mixed layer and the difference (Δday) between the date
518 of observation and the start date of shelf water intrusion at the stations with surface
519 salinity lower than 33. Δday can represent the duration of the shelf water intrusion at
520 each station before our observation. The residence time of O_2 in the mixed layer at most
521 stations listed in Table 3 is shorter than or equivalent to Δday . This result suggests that
522 our estimate has appropriately integrated the NCP during the period of shelf water
523 intrusion, which can effectively reflect the influence of shelf water on productive state
524 on the northern slope of the SCS in the summer.

525 The amount of light may also play a role in the extent of primary production. The
526 MLD is considered a driver of light availability in the mixed layer (Cassar et al., 2011;
527 Hahm et al., 2014). The euphotic layer was averagely 40 m thicker than the mixed layer
528 in the study region during the summer cruise, thus it's not very significant to discuss
529 the light limitation in June 2015. We conducted an analysis of light availability based
530 on daily satellite-PAR data and NCP in October 2014. To minimize the influence of
531 DIN concentrations, we selected 9 stations where surface DIN concentration in the
532 range of 0.10–0.17 $\mu\text{mol L}^{-1}$. The average surface PAR ($\text{mol m}^{-2} \text{d}^{-1}$) at each station
533 was integrated over the residence time of O_2 before our observation. Then an average
534 PAR in the mixed layer was calculated based on K_d . At the selected stations, the surface
535 PAR varies over a range of 38.6–42.2 $\text{mol m}^{-2} \text{d}^{-1}$, while the average PAR in the mixed

536 layer (ML PAR) ranged from 8.7 to 13.3 mol m⁻² d⁻¹ (Table 4). There's no significant
537 correlation between the average PAR and NCP in the mixed layer (Table 4), partly
538 suggesting that light intensity may not be a factor on NCP in the autumn. Light
539 availability in the northern slope region of SCS is enough to support the primary
540 production of phytoplankton.

541

542 **4 Conclusion**

543 The distribution of $\Delta(\text{O}_2/\text{Ar})$ and NCP on the northern slope of the SCS was strongly
544 affected by nutrient availability, especially nitrogen. The nitrogen limitation on NCP
545 was found both in the autumn and summer. In June 2015, we observed strong biological
546 responses to the supply of nitrogen induced by eddy-entrained shelf water intrusion.
547 NCP in the region with the influence of shelf water was 23.8 ± 10.7 mmol C m⁻² d⁻¹ on
548 average, with a maximum of 61.4 mmol C m⁻² d⁻¹. In addition, vertical mixing caused
549 considerable underestimation of NCP in the transect influenced by a cold eddy.
550 Removing the regions with the influence of shelf water intrusion and vertical mixing,
551 the average NCP in other regions was 5.0 ± 6.2 mmol C m⁻² d⁻¹. This value agrees well
552 with previously published NCP estimates for the study area. Our results also reveal the
553 rapid response of ecosystem to physical processes. The summer shelf water intrusion
554 may significantly promote NCP by potentially more than threefold in the study region.
555 This is the first report that quantifies the contribution of shelf water intrusion to NCP
556 on the northern slope of the SCS in the summer. Because of the sufficient illumination
557 in the tropical SCS, light availability may not be a significant limitation on NCP in both
558 seasons. The high-resolution NCP estimates derived from continuous measurement of
559 O₂/Ar presented in this paper are of significance for understanding the carbon cycle in
560 the highly dynamic system of the SCS.

561 **Data Availability**

562 All data presented in this manuscript are available on Weiyun.com (link:
563 <https://share.weiyun.com/ZtbQMNGI>, password: p7rj36)

564 **Author contribution**

565 Guiling Zhang and Yu Han designed and set up the underway measurement system.
566 Wenjing Zheng attended both cruises (in June 2015 and October 2014) in the South
567 China Sea, and was mainly responsible for operating the underway measurement
568 system during the cruises. Sumei Liu provided the nutrients data of both cruises. Chuan
569 Qin attended the cruise in June 2015 and prepared the manuscript with contributions
570 from all co-authors.

571 **Acknowledgments**

572 The authors wish to thank the crew of the *R/V “Nanfeng”* for the assistance with the
573 collection of field samples and Professor Xiaoxia Sun for providing the ^{14}C -PP data.
574 We would also like to thank the Ocean Biology Processing Group (OBPG) of NASA
575 for generating the PAR data and the E.U. Copernicus Marine Environment Monitoring
576 Service (CMEMS) for providing the satellite chlorophyll data. Professor Michael
577 Bender and Bror Jonsson are acknowledged for constructive suggestions on the
578 continuous O_2/Ar measurement system and the calculation of O_2/Ar -based NCP. This
579 study was funded by the National Science Foundation of China through Grant Nos.
580 41776122, by the Ministry of Science and Technology of China through Grant Nos.
581 2014CB441502, by the Fundamental Research Funds for the Central Universities (No.
582 201562010), and by the Taishan Scholars Programme of Shandong Province (No.
583 201511014) and the Aoshan Talents Programme of the Qingdao National Laboratory
584 for Marine Science and Technology (No. 2015ASTP-OS08).

585 **Competing interests**

586 The authors declare that they have no conflict of interest.
587

588 **References:**

- 589 Bi, Q., Du, J., Wu, Y., Zhou, J. and Zhang, J.: Particulate organic carbon export flux by $^{234}\text{Th}/^{238}\text{U}$
590 disequilibrium in the continental slope of the East China Sea, *Acta Oceanol. Sin.*, 32(10), 67–73,
591 doi:10.1007/s13131-013-0303-7, 2013.
- 592 Cai, P., Zhao, D., Wang, L., Huang, B. and Dai, M.: Role of particle stock and phytoplankton
593 community structure in regulating particulate organic carbon export in a large marginal sea, *J.*
594 *Geophys. Res. Oceans*, 120(3), 2063–2095, doi:10.1002/2014JC010432, 2015.
- 595 Cai, W.: Estuarine and Coastal Ocean Carbon Paradox: CO₂ Sinks or Sites of Terrestrial Carbon
596 Incineration?, *Ann. Rev. Mar. Sci.*, 3(1), 123–145, doi:10.1146/annurev-marine-120709-142723,
597 2011.
- 598 Cassar, N., Difiore, P. J., Barnett, B. A., Bender, M. L., Bowie, A. R., Tilbrook, B., Petrou, K.,
599 Westwood, K. J., Wright, S. W. and Lefevre, D.: The influence of iron and light on net community
600 production in the Subantarctic and Polar Frontal Zones, *Biogeosciences*, 8(2), 227–237,
601 doi:10.5194/bg-8-227-2011, 2011.
- 602 Cassar, N., Nevison, C. D. and Manizza, M.: Correcting oceanic O₂/Ar-net community production
603 estimates for vertical mixing using N₂O observations, *Geophys. Res. Lett.*, 41(24), 8961–8970,
604 doi:10.1002/2014GL062040, 2014.
- 605 Chen, J., Zheng, L., Wiesner, M. G., Chen, R., Zheng, Y. and Wong, H.: Estimations of primary
606 production and export production in the South China Sea based on sediment trap experiments,
607 *Chinese Sci. Bull.*, 43(7), 583–586, doi:10.1007/BF02883645, 1998.
- 608 Chen, W., Cai, P., Dai, M. and Wei, J.: $^{234}\text{Th}/^{238}\text{U}$ disequilibrium and particulate organic carbon
609 export in the northern South China Sea, *J. Oceanogr.*, 64(3), 417–428, doi:10.1007/s10872-008-
610 0035-z, 2008.
- 611 Chen, Y. and Tang, D.: Eddy-feature phytoplankton bloom induced by a tropical cyclone in the
612 South China Sea, *Int. J. Remote Sens.*, 33(23), 7444–7457, doi:10.1080/01431161.2012.685976,
613 2012.
- 614 Chen, Z., Yang, C., Xu, D. and Xu, M.: Observed hydrographical features and circulation with
615 influences of cyclonic-anticyclonic eddy-pair in the northern slope of the South China Sea during
616 June 2015 (in Chinese), *J. Mar. Sci.*, 34(4), 10–19, doi:10.3969/j.issn.1001-909X.2016.04.002,

617 2016.

618 Cheng, G., Sun, J., Zu, T., Chen, J. and Wang, D.: Analysis of water masses in the northern South
619 China Sea in summer 2011 (in Chinese), *J. Trop. Oceanogr.*, 33(3), 10–16, doi:10.3969/j.issn.1009-
620 5470.2014.03.002, 2014.

621 Chou, W., Lee Chen, Y., Sheu, D., Shih, Y., Han, C., Cho, C., Tseng, C. and Yang, Y.: Estimated
622 net community production during the summertime at the SEATS time-series study site, northern
623 South China Sea: Implications for nitrogen fixation, *Geophys. Res. Lett.*, 33(22),
624 doi:10.1029/2005GL025365, 2006.

625 Clark, D. R., Rees, A. P. and Joint, I.: Ammonium regeneration and nitrification rates in the
626 oligotrophic Atlantic Ocean: Implications for new production estimates, *Limnol. Oceanogr.*, 53(1),
627 52–62, doi:10.4319/lo.2008.53.1.0052, 2008.

628 Craig, H. and Hayward, T.: Oxygen Supersaturation in the Ocean: Biological Versus Physical
629 Contributions, *Science*, 235(4785), 199–202, doi:10.1126/science.235.4785.199, 1987.

630 Dugdale, R. C. and Goering, J. J.: Uptake of New and Regenerated Forms of Nitrogen in Primary
631 Productivity, *Limnol. Oceanogr.*, 12(2), 196–206, doi:10.4319/lo.1967.12.2.0196, 1967.

632 Emerson, S., Quay, P., Stump, C., Wilbur, D. and Knox, M.: O₂, Ar, N₂, and ²²²Rn in surface waters
633 of the subarctic Ocean: Net biological O₂ production, *Global Biogeochem. Cycles*, 5(1), 49–69,
634 doi:10.1029/90GB02656, 1991.

635 Eveleth, R., Cassar, N., Sherrell, R. M., Ducklow, H., Meredith, M. P., Venables, H. J., Lin, Y. and
636 Li, Z.: Ice melt influence on summertime net community production along the Western Antarctic
637 Peninsula, *Deep Sea Res. Part II Top. Stud. Oceanogr.*, 139, 89–102,
638 doi:10.1016/j.dsr2.2016.07.016, 2017.

639 Fan, L., Su, Y. and Li, F.: Analysis on water masses in the Northern South China Sea (in Chinese),
640 *Acta Oceanol. Sin.*, 10(2), 136–145, 1988.

641 Feng, S., Li, F. and Li, S.: An introduction to marine science (in Chinese), Higher Education Press,
642 Beijing, China., 1999.

643 Giesbrecht, K. E., Hamme, R. C. and Emerson, S. R.: Biological productivity along Line P in the
644 subarctic northeast Pacific: In situ versus incubation-based methods, *Global Biogeochem. Cycles*,
645 26(3), doi:10.1029/2012GB004349, 2012.

646 Grande, K. D., Williams, P. J. L. B., Marra, J., Purdie, D. A., Heinemann, K., Eppley, R. W. and

647 Bender, M. L.: Primary production in the North Pacific gyre: a comparison of rates determined by
648 the ^{14}C , O_2 concentration and ^{18}O methods, *Deep Sea Res. Part A, Oceanogr. Res. Pap.*, 36(11),
649 1621–1634, doi:10.1016/0198-0149(89)90063-0, 1989.

650 Guéguen, C. and Tortell, P. D.: High-resolution measurement of Southern Ocean CO_2 and O_2/Ar by
651 membrane inlet mass spectrometry, *Mar. Chem.*, 108(3–4), 184–194,
652 doi:10.1016/j.marchem.2007.11.007, 2008.

653 Hahm, D., Rhee, T. S., Kim, H. C., Park, J., Kim, Y. N., Shin, H. C. and Lee, S.: Spatial and temporal
654 variation of net community production and its regulating factors in the Amundsen Sea, Antarctica,
655 *J. Geophys. Res. Oceans*, 119(5), 2815–2826, doi:10.1002/2013JC009762, 2014.

656 Hamme, R. C., Cassar, N., Lance, V. P., Vaillancourt, R. D., Bender, M. L., Strutton, P. G., Moore,
657 T. S., DeGrandpre, M. D., Sabine, C. L., Ho, D. T. and Hargreaves, B. R.: Dissolved O_2/Ar and
658 other methods reveal rapid changes in productivity during a Lagrangian experiment in the Southern
659 Ocean, *J. Geophys. Res. Oceans*, 117(C4), 92–99, doi:10.1029/2011JC007046, 2012.

660 Han, A., Dai, M., Gan, J., Kao, S., Zhao, X., Jan, S., Li, Q., Lin, H., Chen, C., Wang, L., Hu, J.,
661 Wang, L. and Gong, F.: Inter-shelf nutrient transport from the East China Sea as a major nutrient
662 source supporting winter primary production on the northeast South China Sea shelf,
663 *Biogeosciences*, 10(12), 8159–8170, doi:10.5194/bg-10-8159-2013, 2013.

664 Hanson, C. E., Pesant, S., Waite, A. M. and Pattiaratchi, C. B.: Assessing the magnitude and
665 significance of deep chlorophyll maxima of the coastal eastern Indian Ocean, *Deep. Res. Part II Top.*
666 *Stud. Oceanogr.*, 54(8–10), 884–901, doi:10.1016/j.dsr2.2006.08.021, 2007.

667 He, X., Xu, D., Bai, Y., Pan, D., Chen, C. A., Chen, X. and Gong, F.: Eddy-entrained Pearl River
668 plume into the oligotrophic basin of the South China Sea, *Cont. Shelf Res.*, 124, 117–124,
669 doi:10.1016/j.csr.2016.06.003, 2016.

670 Hendricks, M. B., Bender, M. L. and Barnett, B. A.: Net and gross O_2 production in the southern
671 ocean from measurements of biological O_2 saturation and its triple isotope composition, *Deep. Res.*
672 *Part I Oceanogr. Res. Pap.*, 51(11), 1541–1561, doi:10.1016/j.dsr.2004.06.006, 2004.

673 Hu, J., Kawamura, H., Hong, H. and Qi, Y.: A Review on the currents in the South China Sea:
674 Seasonal circulation, South China Sea warm current and Kuroshio intrusion, *J. Oceanogr.*, 56(6),
675 607–624, doi:10.1023/A:1011117531252, 2000.

676 Huang, K., Ducklow, H., Vernet, M., Cassar, N. and Bender, M. L.: Export production and its

677 regulating factors in the West Antarctica Peninsula region of the Southern Ocean, *Global*
678 *Biogeochem. Cycles*, 26(2), doi:10.1029/2010GB004028, 2012.

679 Huang, Y., Yang, B., Chen, B., Qiu, G., Wang, H. and Huang, B.: Net community production in the
680 South China Sea Basin estimated from in situ O₂ measurements on an Argo profiling float, *Deep*
681 *Sea Res. Part I Oceanogr. Res. Pap.*, 131, 54–61, doi:10.1016/j.dsr.2017.11.002, 2018.

682 Izett, R. W., Manning, C. C., Hamme, R. C. and Tortell, P. D.: Refined Estimates of Net Community
683 Production in the Subarctic Northeast Pacific Derived From $\Delta\text{O}_2/\text{Ar}$ Measurements With N₂O-
684 Based Corrections for Vertical Mixing, *Global Biogeochem. Cycles*, 32(3), 326–350,
685 doi:10.1002/2017GB005792, 2018.

686 Jiang, Z., Huang, C., Dai, M., Kao, S., Hydes, D. J., Chou, W. and Janf, S.: Short-term dynamics of
687 oxygen and carbon in productive nearshore shallow seawater systems off Taiwan: Observations and
688 modeling, *Limnol. Oceanogr.*, 56(5), 1832–1849, doi:10.4319/lo.2011.56.5.1832, 2011.

689 Jonsson, B. F., Doney, S. C., Dunne, J. and Bender, M.: Evaluation of the Southern Ocean O₂/Ar-
690 based NCP estimates in a model framework, *J. Geophys. Res. Biogeosciences*, 118(2), 385–399,
691 doi:10.1002/jgrg.20032, 2013.

692 Jerlov, N. G.: *Marine optics*, Elsevier, Netherlands, 1976.

693 Kaiser, J., Reuer, M. K., Barnett, B. and Bender, M. L.: Marine productivity estimates from
694 continuous O₂/Ar ratio measurements by membrane inlet mass spectrometry, *Geophys. Res. Lett.*,
695 32(19), 1–5, doi:10.1029/2005GL023459, 2005.

696 Kirk, J. T.: *Light and photosynthesis in aquatic ecosystems*, Cambridge university press, UK, 1994.

697 La Roche, J.: Ammonium regeneration: its contribution to phytoplankton nitrogen requirements in
698 a eutrophic environment, *Mar. Biol.*, 75(2–3), 231–240, doi:10.1007/BF00406007, 1983.

699 Lee Chen, Y.: Spatial and seasonal variations of nitrate-based new production and primary
700 production in the South China Sea, *Deep Sea Res. Part I Oceanogr. Res. Pap.*, 52(2), 319–340,
701 doi:10.1016/j.dsr.2004.11.001, 2005.

702 Lee Chen, Y. and Chen, H.: Seasonal dynamics of primary and new production in the northern South
703 China Sea: The significance of river discharge and nutrient advection, *Deep Sea Res. Part I*
704 *Oceanogr. Res. Pap.*, 53(6), 971–986, doi:10.1016/j.dsr.2006.02.005, 2006.

705 Li, D., Zhou, M., Zhang, Z., Zhong, Y., Zhu, Y., Yang, C., Xu, M., Xu, D. and Hu, Z.: Intrusions
706 of Kuroshio and Shelf Waters on Northern Slope of South China Sea in Summer 2015, *J. Ocean*

707 Univ. China, 17(3), 477–486, doi:10.1007/s11802-018-3384-2, 2018.

708 Li, Q., Guo, X., Zhai, W., Xu, Y. and Dai, M.: Partial pressure of CO₂ and air-sea CO₂ fluxes in the
709 South China Sea: Synthesis of an 18-year dataset, Prog. Oceanogr., 182,
710 doi:10.1016/j.pocean.2020.102272, 2020.

711 Liao, X., Dai, M., Gong, X., Liu, X. and Huang, H.: Subsurface chlorophyll a maximum and its
712 possible causes in the southern South China Sea, J. Trop. Oceanogr., 37(1), 45–56,
713 doi:10.11978/2017020, 2018.

714 Lin, X., Guan, Y. and Liu, Y.: Three-dimensional structure and evolution process of Dongsha Cold
715 Eddy during autumn 2000 (in Chinese), J. Trop. Oceanogr., 32(2), 55–65, doi:10.3969/j.issn.1009-
716 5470.2013.02.006, 2013.

717 Liu, M., Liu, X., Ma, A., Li, T. and Du, Z.: Spatio-temporal stability and abnormality of chlorophyll-
718 a in the northern south china sea during 2002-2012 from MODIS images using wavelet analysis,
719 Cont. Shelf Res., 75, 15–27, doi:10.1016/j.csr.2013.12.010, 2014.

720 Lockwood, D., Quay, P. D., Kavanaugh, M. T., Juranek, L. W. and Feely, R. A.: High-resolution
721 estimates of net community production and air-sea CO₂ flux in the northeast Pacific, Global
722 Biogeochem. Cycles, 26(4), doi:10.1029/2012GB004380, 2012.

723 Ma, H., Zeng, Z., He, J., Chen, L., Yin, M., Zeng, S. and Zeng, W.: Vertical flux of particulate
724 organic carbon in the central South China Sea estimated from ²³⁴Th-²³⁸U disequilibria, Chinese J.
725 Oceanol. Limnol., 26(4), 480–485, doi:10.1007/s00343-008-0480-y, 2008.

726 Ma, H., Zeng, Z., Yu, W., He, J., Chen, L., Cheng, J., Yin, M. and Zeng, S.: ²³⁴Th/ ²³⁸U
727 disequilibrium and particulate organic carbon export in the northwestern South China Sea, Acta
728 Oceanol. Sin., 30(3), 55–62, doi:10.1007/s13131-011-0119-2, 2011.

729 Manning, C. C., Stanley, R. H. R., Nicholson, D. P., Smith, J. M., Timothy Pennington, J., Fewings,
730 M. R., Squibb, M. E. and Chavez, F. P.: Impact of recently upwelled water on productivity
731 investigated using in situ and incubation-based methods in Monterey Bay, J. Geophys. Res. Oceans,
732 122(3), 1901–1926, doi:10.1002/2016JC012306, 2017.

733 Mathis, J. T., Cross, J. N. and Bates, N. R.: Coupling primary production and terrestrial runoff to
734 ocean acidification and carbonate mineral suppression in the eastern Bering Sea, J. Geophys. Res.
735 Ocean., 116(2), doi:10.1029/2010JC006453, 2011.

736 Millero, F. J. and Poisson, A.: International one-atmosphere equation of state of seawater, Deep Sea

737 Res. Part A, Oceanogr. Res. Pap., 28(6), 625–629, doi:10.1016/0198-0149(81)90122-9, 1981.

738 Monterey, G. and Levitus, S.: Seasonal Variability of Mixed Layer Depth, NOAA Atlas NEDIS 14,
739 U.S. Gov. Printing Off. D.C. [online] Available from: <http://www.nodc.noaa.gov>, 1997.

740 NASA Goddard Space Flight Center, Ocean Ecology Laboratory, Ocean Biology Processing Group:
741 Moderate-resolution Imaging Spectroradiometer (MODIS) Aqua Photosynthetically Available
742 Radiation Data, NASA OB. DAAC, Greenbelt, MD, USA. doi:
743 data/10.5067/AQUA/MODIS/L3M/PAR/2018, 2018 Reprocessing.

744 Nemcek, N., Ianson, D. and Tortell, P. D.: A high-resolution survey of DMS, CO₂, and O₂/Ar
745 distributions in productive coastal waters, Global Biogeochem. Cycles, 22(2),
746 doi:10.1029/2006GB002879, 2008.

747 Ning, X., Chai, F., Xue, H., Cai, Y., Liu, C. and Shi, J.: Physical-biological oceanographic coupling
748 influencing phytoplankton and primary production in the South China Sea, J. Geophys. Res. Oceans,
749 109(10), doi:10.1029/2004JC002365, 2004.

750 Ning, X., Peng, X., Le, F., Hao, Q., Sun, J., Liu, C. and Cai, Y.: Nutrient limitation of phytoplankton
751 in anticyclonic eddies of the northern South China Sea, Biogeosciences Discuss., 5(6), 4591–4619,
752 doi:10.5194/bgd-5-4591-2008, 2008.

753 Pan, X., Wong, G. T. F., Shiah, F. K. and Ho, T. Y.: Enhancement of biological productivity by
754 internal waves: Observations in the summertime in the northern South China Sea, J. Oceanogr.,
755 68(3), 427–437, doi:10.1007/s10872-012-0107-y, 2012.

756 Parsons, T. R., Maita, Y. and Lalli, C. M.: A Manual of Chemical & Biological Methods for
757 Seawater Analysis, Pergamon Press, Oxford, UK., 1984.

758 Pawlowicz, R.: M_Map: A mapping package for MATLAB, version 1.4m, [online] Available from:
759 www.eoas.ubc.ca/~rich/map.html, 2020.

760 Quay, P. D., Peacock, C., Bjrkman, K. and Karl, D. M.: Measuring primary production rates in the
761 ocean: Enigmatic results between incubation and non-incubation methods at Station ALOHA,
762 Global Biogeochem. Cycles, 24(3), doi:10.1029/2009GB003665, 2010.

763 Rehder, G. and Suess, E.: Methane and pCO₂ in the Kuroshio and the South China Sea during
764 maximum summer surface temperatures, Mar. Chem., 75(1–2), 89–108, doi:10.1016/S0304-
765 4203(01)00026-3, 2001.

766 Reuer, M. K., Barnett, B. A., Bender, M. L., Falkowski, P. G. and Hendricks, M. B.: New estimates

767 of Southern Ocean biological production rates from O₂/Ar ratios and the triple isotope composition
768 of O₂, *Deep Sea Res. Part I Oceanogr. Res. Pap.*, 54(6), 951–974, doi:10.1016/j.dsr.2007.02.007,
769 2007.

770 Shadwick, E. H., Tilbrook, B., Cassar, N., Trull, T. W. and Rintoul, S. R.: Summertime physical
771 and biological controls on O₂ and CO₂ in the Australian Sector of the Southern Ocean, *J. Mar. Syst.*,
772 147, 21–28, doi:10.1016/j.jmarsys.2013.12.008, 2015.

773 Shi, X., Li, H., Han, X., Wang, L. and Zhu, C.: Influence of typical mesoscale oceanographical
774 process on the distribution of nutrients and dissolved oxygen in the Northern part of South China
775 Sea in summer (in Chinese), *Acta Sci. Circumstantiae*, 34(3), 695–703,
776 doi:10.13671/j.hjkxxb.2014.0121, 2014.

777 Stanley, R. H. R., Kirkpatrick, J. B., Cassar, N., Barnett, B. A. and Bender, M. L.: Net community
778 production and gross primary production rates in the western equatorial Pacific, *Global Biogeochem.*
779 *Cycles*, 24(4), doi:10.1029/2009GB003651, 2010.

780 Su, J. and Yuan, Y.: *Coastal hydrology of China* (in Chinese), China Ocean Press, Beijing, China.,
781 2005.

782 Takahashi, T., Sutherland, S. C., Wanninkhof, R., Sweeney, C., Feely, R. A., Chipman, D. W.,
783 Hales, B., Friederich, G., Chavez, F., Sabine, C., Watson, A., Bakker, D. C. E., Schuster, U., Metzl,
784 N., Yoshikawa-Inoue, H., Ishii, M., Midorikawa, T., Nojiri, Y., Körtzinger, A., Steinhoff, T.,
785 Hoppema, M., Olafsson, J., Arnarson, T. S., Tilbrook, B., Johannessen, T., Olsen, A., Bellerby, R.,
786 Wong, C. S., Delille, B., Bates, N. R. and de Baar, H. J. W.: Climatological mean and decadal
787 change in surface ocean *p*CO₂, and net sea–air CO₂ flux over the global oceans, *Deep Sea Res. Part*
788 *II Top. Stud. Oceanogr.*, 56(8–10), 554–577, doi:10.1016/j.dsr2.2008.12.009, 2009.

789 Tamminen, T.: Effects of ammonium effluents on planktonic primary production and
790 decomposition in a coastal brackish water environment I. Nutrient balance of the water body and
791 effluent tests, *Netherlands J. Sea Res.*, 16(C), 455–464, doi:10.1016/0077-7579(82)90050-3, 1982.

792 Teeter, L., Hamme, R. C., Ianson, D. and Bianucci, L.: Accurate Estimation of Net Community
793 Production From O₂/Ar Measurements, *Global Biogeochem. Cycles*, 32(8), 1163–1181,
794 doi:10.1029/2017GB005874, 2018.

795 Teira, E., Mouriño, B., Marañón, E., Pérez, V., Pazó, M. J., Serret, P., De Armas, D., Escáñez, J.,
796 Woodward, E. M. S. and Fernández, E.: Variability of chlorophyll and primary production in the

797 Eastern North Atlantic Subtropical Gyre: Potential factors affecting phytoplankton activity, *Deep.*
798 *Res. Part I Oceanogr. Res. Pap.*, 52(4), 569–588, doi:10.1016/j.dsr.2004.11.007, 2005.

799 Tortell, P. D.: Dissolved gas measurements in oceanic waters made by membrane inlet mass
800 spectrometry, *Limnol. Oceanogr. Methods*, 3(1), 24–37, doi:10.4319/lom.2005.3.24, 2005.

801 Tortell, P. D., Asher, E. C., Ducklow, H. W., Goldman, J. A. L., Dacey, J. W. H., Grzymiski, J. J.,
802 Young, J. N., Kranz, S. A., Bernard, K. S. and Morel, F. M. M.: Metabolic balance of coastal
803 Antarctic waters revealed by autonomous $p\text{CO}_2$ and $\Delta\text{O}_2/\text{Ar}$ measurements, *Geophys. Res. Lett.*,
804 41(19), 6803–6810, doi:10.1002/2014GL061266, 2014.

805 Tortell, P. D., Merzouk, A., Ianson, D., Pawlowicz, R. and Yelland, D. R.: Influence of regional
806 climate forcing on surface water $p\text{CO}_2$, $\Delta\text{O}_2/\text{Ar}$ and dimethylsulfide (DMS) along the southern
807 British Columbia coast, *Cont. Shelf Res.*, 47, 119–132, doi:10.1016/j.csr.2012.07.007, 2012.

808 Ulfso, A., Cassar, N., Korhonen, M., Van Heuven, S., Hoppema, M., Kattner, G. and Anderson, L.
809 G.: Late summer net community production in the central Arctic Ocean using multiple approaches,
810 *Global Biogeochem. Cycles*, 28(10), 1129–1148, doi:10.1002/2014GB004833, 2014.

811 Uu, D. V. and Brankart, J. M.: Seasonal variation of temperature and salinity fields and water masses
812 in the Bien Dong (South China) Sea, *Math. Comput. Model.*, 26(12), 97–113, doi:10.1016/S0895-
813 7177(97)00243-4, 1997.

814 Wang, N., Lin, W., Cheng, B. and Huang, B.: Metabolic states of the Taiwan Strait and the northern
815 South China Sea in summer 2012 (in Chinese), *J. Trop. Oceanogr.*, 33(4), 61–68,
816 doi:10.3969/j.issn.1009-5470.2014.04.008, 2014.

817 Wanninkhof, R.: Relationship between wind speed and gas exchange over the ocean, *J. Geophys.*
818 *Res. Oceans*, 97(C5), 7373–7382, doi:10.1029/92JC00188, 1992.

819 Weiss, R. F.: The solubility of nitrogen, oxygen and argon in water and seawater, *Deep Sea Res.*
820 *Oceanogr. Abstr.*, 17(4), 721–735, doi:10.1016/0011-7471(70)90037-9, 1970.

821 Zhai, W., Dai, M. and Cai, W.: Coupling of surface $p\text{CO}_2$ and dissolved oxygen in the northern
822 South China Sea: Impacts of contrasting coastal processes, *Biogeosciences*, 6(11), 2589–2598,
823 doi:10.5194/bg-6-2589-2009, 2009.

824 Zhang, R., Zhu, X., Yang, C., Ye, L., Zhang, G., Ren, J., Wu, Y., Liu, S., Zhang, J. and Zhou, M.:
825 Distribution of dissolved iron in the Pearl River (Zhujiang) Estuary and the northern continental
826 slope of the South China Sea, *Deep. Res. Part II Top. Stud. Oceanogr.*, 167, 14–24,

827 doi:10.1016/j.dsr2.2018.12.006, 2019.

828

829

830 **Table Captions:**

831 **Table 1.** Basic information at all CTD stations in October 2014

832 **Table 2.** Basic information at all CTD stations in June 2015

833 **Table 3.** The start date and duration (Δ day) of shelf water intrusion at the stations with surface
834 salinity lower than 33 in June 2015

835 **Table 4.** Satellite-PAR data and NCP at the selected stations in October 2014

836

837 **Figure Captions:**

838 **Figure 1.** Cruise tracks of two cruises in the slope region of the Northern South China Sea in (a)
839 October 2014, (b) June 2015. The sea level height anomaly (SLA) and geostrophic current during
840 observations in June 2015 (Chen et al., 2016) are shown in (c). The black dots/stars represent the
841 locations of the CTD casts. Red numbers indicate transects, while black numbers indicate the serial
842 number of CTD stations based on the cruise plan. The color scale in (a) and (b) represents
843 bathymetry.

844 **Figure 2.** Surface distributions of (a) temperature, (b) salinity, (c) chlorophyll-a (Chl a), and (d)
845 $\Delta(\text{O}_2/\text{Ar})$ in October 2014

846 **Figure 3.** Surface distributions of (a) temperature, (b) salinity, (c) chlorophyll-a (Chl a), (d)
847 dissolved oxygen (DO), (e) $p\text{CO}_2$, and (f) $\Delta(\text{O}_2/\text{Ar})$ in June 2015

848 **Figure 4.** Surface distribution of NCP among the northern slope of SCS during the cruise in (a)
849 October 2014 and (b) June 2015.

850 **Figure 5.** Zonal variations in (a) temperature, salinity, (b) $\Delta(\text{O}_2/\text{Ar})$, (c) Chl a, NCP and surface
851 concentration of ammonia (NH_4^+) along Transect 5 in October 2014. The plots of $\Delta(\text{O}_2/\text{Ar})$ and NCP
852 are 10-point Savitzky-Golay smoothed to give a better view of their distribution.

853 **Figure 6.** Meridional variations in (a) temperature, salinity, (b) $\Delta(\text{O}_2/\text{Ar})$, $p\text{CO}_2$, (c) Chl a, NCP and
854 surface concentration of DIN along Transect 4 in June 2015. The plots of $\Delta(\text{O}_2/\text{Ar})$, $p\text{CO}_2$ and NCP
855 are 10-point Savitzky-Golay smoothed.

856 **Figure 7.** Principal Component Analysis (PCA) among variables for (a) October 2014 and (b) June
857 2015 (Bartlett's test of sphericity: $p < 0.01$)

858 **Figure 8.** (a) T-S diagram of surface DIN concentration in June 2015. The stations influenced by
859 shelf water were in the red circle. (b) Correlation analysis between surface DIN concentration and
860 NCP at sampling stations. The stations (characterized with $S < 33$) influenced by shelf water
861 presented surface DIN concentration $\geq 0.27 \mu\text{mol L}^{-1}$.

862 **Figure 9.** Correlation analysis between underway NCP and physical parameters (temperature and
863 salinity) in October 2014 (a, b) and June 2015 (c, d).

864 **Figure 10.** Daily satellite-chlorophyll images on the selected days in June 2015. Stars represent
865 CTD locations. We roughly set satellite-chlorophyll $\geq 0.2 \mu\text{g L}^{-1}$ in this figure as the criterion of

866 shelf water. This figure was made based on the M_Map mapping package for MATLAB (Pawlowicz,
867 2020).

Table 1. Basic information at all CTD stations in October 2014

Station	Date of observation ^a	MLD (m)	Z _{eu} ^b (m)	k ^c (m d ⁻¹)	τ ^d (d)
O-01	13 Oct 2014	58	82	4.7	12
O-02	13 Oct 2014	64	74	5.2	12
O-03	14 Oct 2014	56	84	6.2	9
O-04	14 Oct 2014	54	76	6.3	9
O-05	20 Oct 2014	27	70	7.9	3
O-06	19 Oct 2014	55	62	8.4	7
O-07	21 Oct 2014	40	60	7.3	5
O-08	21 Oct 2014	49	72	7.4	7
O-09	15 Oct 2014	79	96	6.2	13
O-10	15 Oct 2014	68	81	6.1	11
O-11	15 Oct 2014	64	81	5.4	12
O-12	16 Oct 2014	66	74	5.2	13
O-13	16 Oct 2014	48	52	6.3	8
O-14	17 Oct 2014	54	62	6.9	8
O-15	22 Oct 2014	49	68	7.0	7
O-16	22 Oct 2014	50	73	7.3	7
O-17	23 Oct 2014	52	75	7.9	7
O-19	18 Oct 2014	31	64	9.4	3
O-20	18 Oct 2014	35	61	8.7	4
O-21	18 Oct 2014	81	86	6.9	12
O-22	17 Oct 2014	76	102	6.0	13

^a All dates are in the format of day month year. ^b Euphotic depth, defined based on subsurface chlorophyll maximum layer. ^c Gas transfer velocity of O₂. ^d Residence time of O₂ in the mixed layer, estimated as per MLD/k.

868

Table 2. Basic information at all CTD stations in June 2015

Station	Date of observation	MLD (m)	Z_{eu} (m)	k (m d⁻¹)	τ (d)
J-01	18 Jun 2015	26	63	2.2	12
J-02	17 Jun 2015	19	80	1.9	10
J-03	16 Jun 2015	20	74	1.9	11
J-04	15 Jun 2015	22	74	1.9	11
J-05	15 Jun 2015	11	78	1.2	9
J-06	14 Jun 2015	24	76	2.1	11
J-07	13 Jun 2015	21	81	2.3	9
J-08	18 Jun 2015	14	56	1.7	8
J-09	19 Jun 2015	17	59	1.6	10
J-10	19 Jun 2015	8	46	1.4	6
J-11	20 Jun 2015	8	40	2.8	3
J-12	21 Jun 2015	16	45	3.0	5
J-13	21 Jun 2015	19	45	2.3	8
J-14	24 Jun 2015	28	55	4.0	7
J-15	24 Jun 2015	17	42	5.3	3
J-16	25 Jun 2015	10	19	5.7	2

869

870

871
872
873

Table 3. The start date and duration (Δ day) of shelf water intrusion at the stations with surface salinity lower than 33 in June 2015

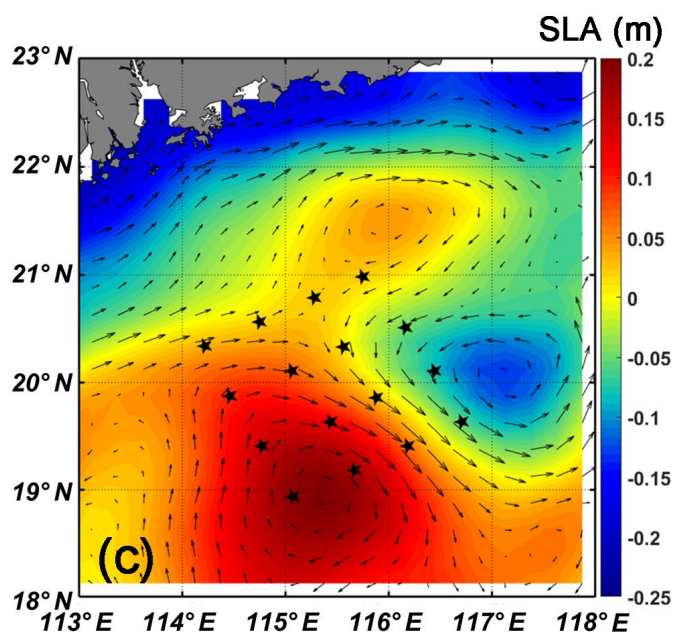
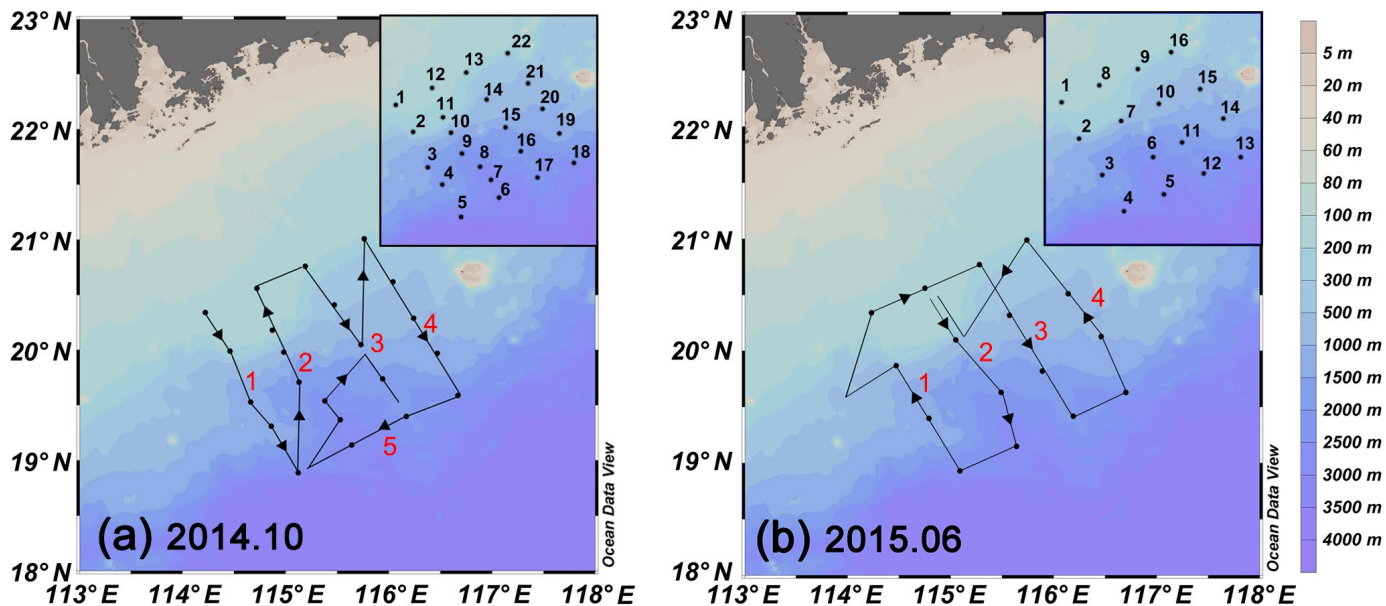
Station	Date of observation	Start date of shelf water intrusion	Δ day ^a	τ (d)
J-09	19 Jun 2015	10 Jun 2015	9	10
J-10	19 Jun 2015	13 Jun 2015	6	6
J-11	20 Jun 2015	13 Jun 2015	7	3
J-12	21 Jun 2015	13 Jun 2015	8	5
J-13	21 Jun 2015	13 Jun 2015	8	8
J-16	25 Jun 2015	before 10 Jun 2015	> 15	2

^a The difference between the date of observation and the start date of shelf water intrusion at listed stations.

Table 4. Satellite-PAR data and NCP at the selected stations in October 2014

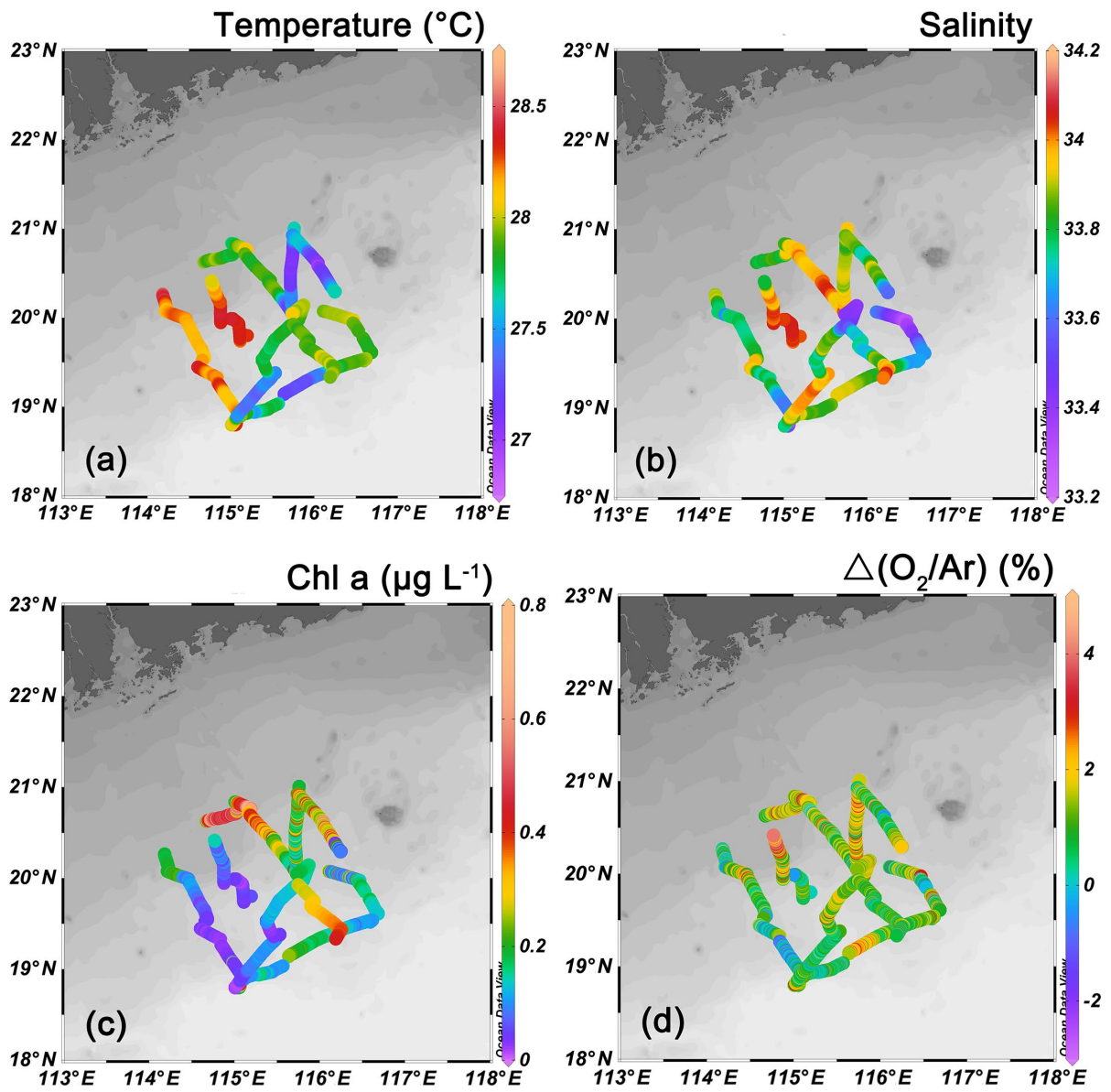
Station	Date of observation	MLD (m)	Z_{eu} (m)	Surface PAR^a (mol m⁻² d⁻¹)	K_d (m⁻¹)	ML PAR^b (mol m⁻² d⁻¹)	NCP (mmol C m⁻² d⁻¹)
O-01	13 Oct 2014	58	82	42.0	5.6 * 10 ⁻²	12.0	3.0
O-02	13 Oct 2014	64	74	42.0	6.2 * 10 ⁻²	10.0	15.1
O-03	14 Oct 2014	56	84	41.1	5.5 * 10 ⁻²	12.4	10.1
O-08	21 Oct 2014	49	72	38.7	6.4 * 10 ⁻²	11.4	15.7
O-10	15 Oct 2014	68	81	40.0	5.7 * 10 ⁻²	9.8	4.4
O-13	16 Oct 2014	48	52	39.2	8.9 * 10 ⁻²	8.7	15.3
O-15	22 Oct 2014	49	68	38.6	6.8 * 10 ⁻²	10.8	16.3
O-20	18 Oct 2014	35	61	39.2	7.5 * 10 ⁻²	13.3	16.4
O-22	17 Oct 2014	76	102	42.2	4.5 * 10 ⁻²	11.6	15.7

^a Average surface PAR over the residence time of O₂ in the mixed layer. ^b Average PAR in the mixed layer.

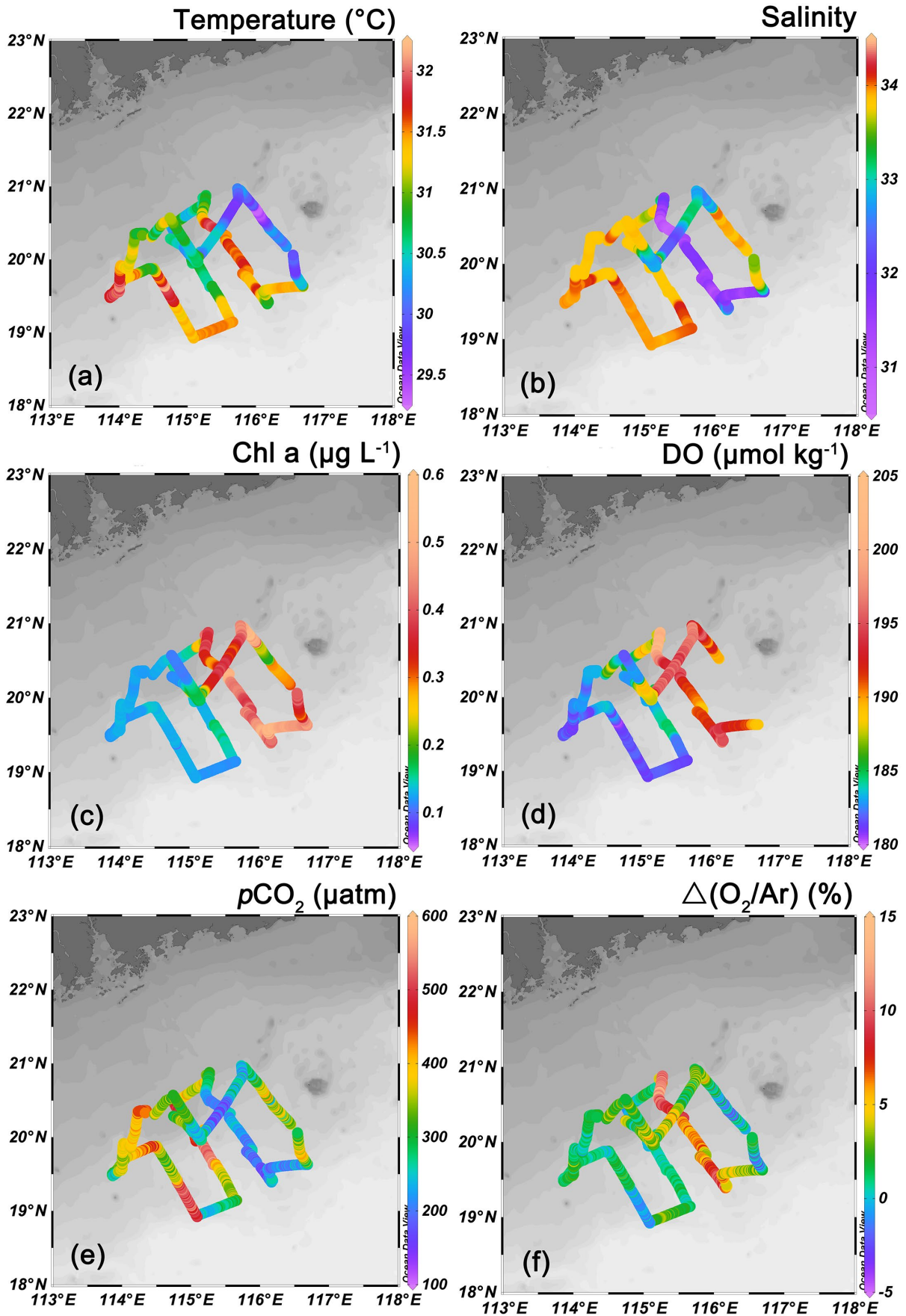


875
876
877
878
879
880

Figure 1. Cruise tracks of two cruises in the slope region of the Northern South China Sea in (a) October 2014, (b) June 2015. The sea level height anomaly (SLA) and geostrophic current during observations in June 2015 (Chen et al., 2016) are shown in (c). The black dots/stars represent the locations of the CTD casts. Red numbers indicate transects, while black numbers indicate the serial number of CTD stations based on the cruise plan. The color scale in (a) and (b) represents bathymetry.



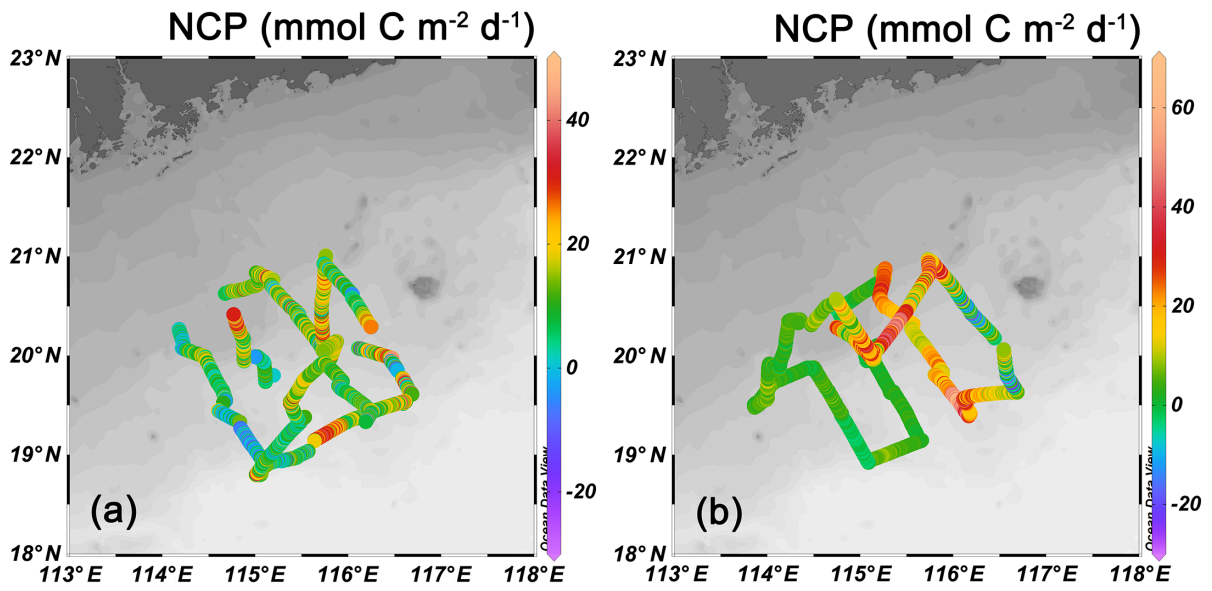
881
882 **Figure 2.** Surface distributions of (a) temperature, (b) salinity, (c) chlorophyll-a (Chl a), and (d) $\Delta(\text{O}_2/\text{Ar})$ in October 2014
883
884



885
886 **Figure 3.** Surface distributions of (a) temperature, (b) salinity, (c) chlorophyll-a (Chl a), (d) dissolved oxygen (DO), (e)

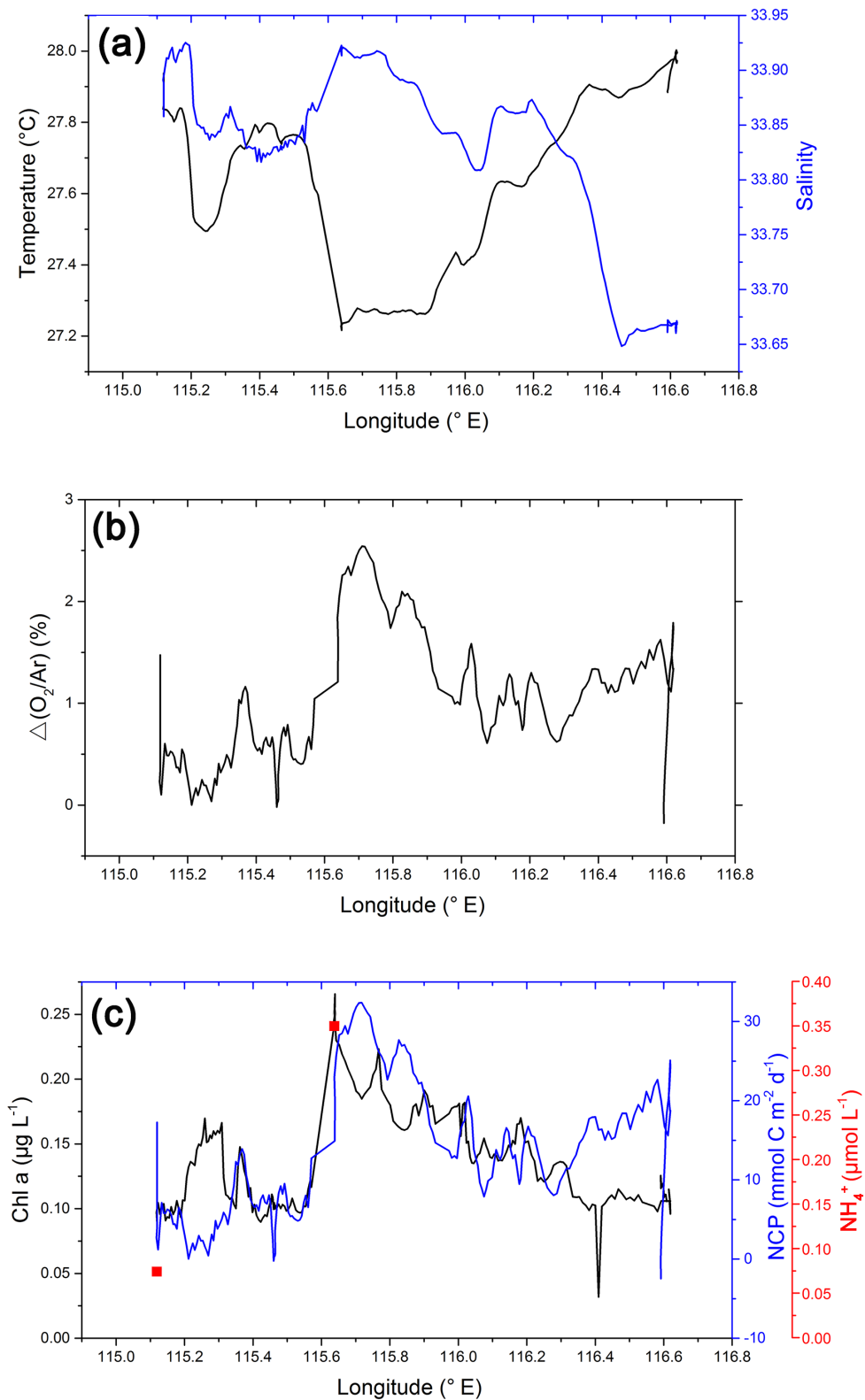
887 $p\text{CO}_2$, and (f) $\Delta(\text{O}_2/\text{Ar})$ in June 2015

888



889
 890 **Figure 4.** Surface distribution of NCP among the northern slope of SCS during the cruise in **(a)** October 2014 and **(b)** June
 891 2015.

891
 892
 893



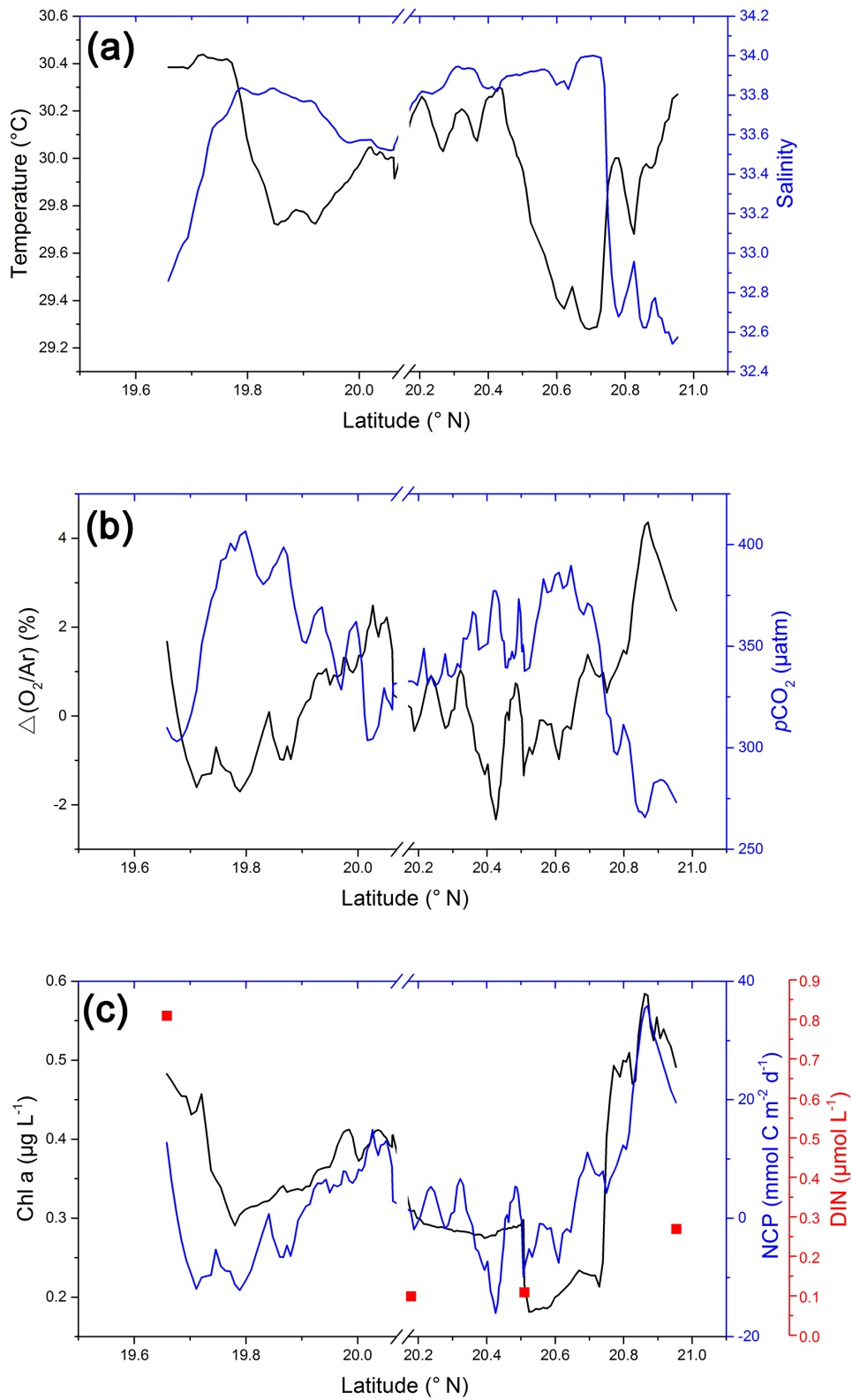
894

895

896

897

Figure 5. Zonal variations in (a) temperature, salinity, (b) $\Delta(\text{O}_2/\text{Ar})$, (c) Chl a, NCP and surface concentration of ammonia (NH_4^+) along Transect 5 in October 2014. The plots of $\Delta(\text{O}_2/\text{Ar})$ and NCP are 10-point Savitzky-Golay smoothed to give a better view of their distribution.



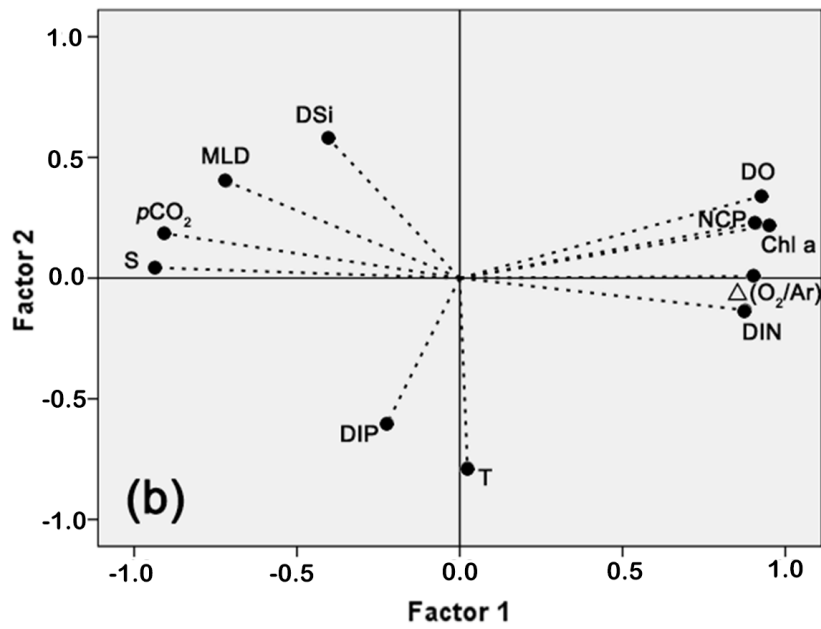
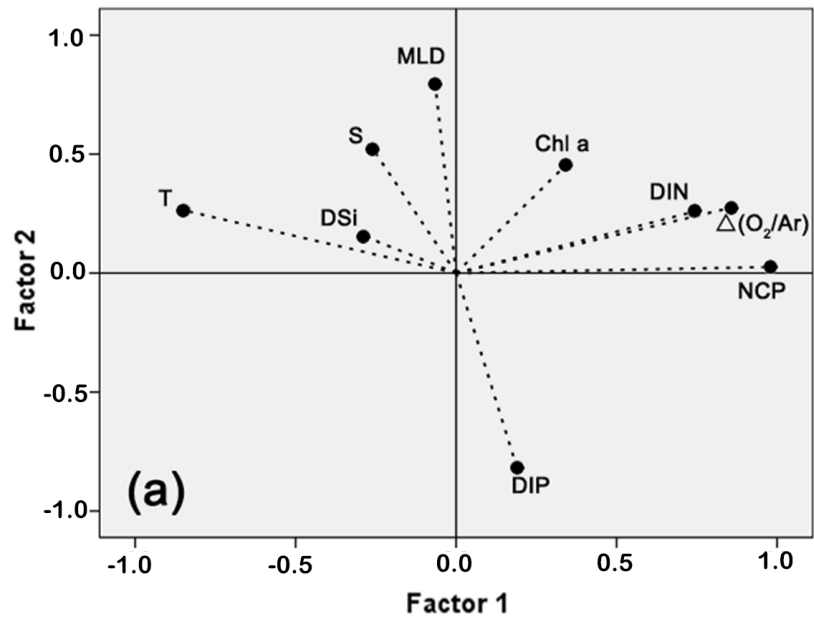
898

899

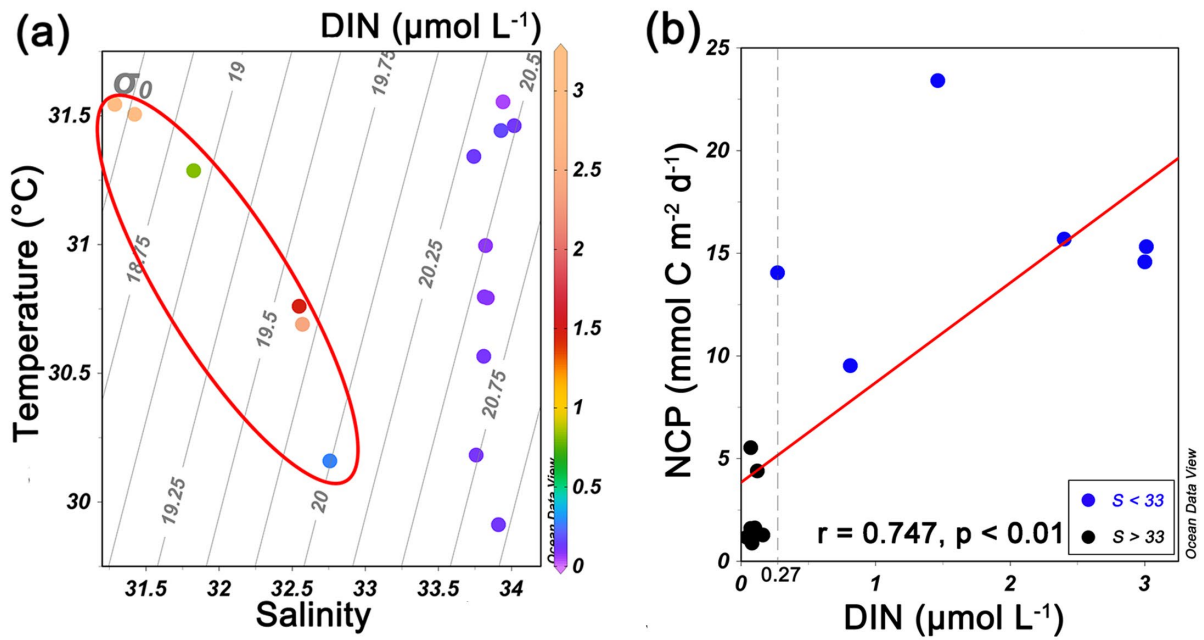
Figure 6. Meridional variations in **(a)** temperature, salinity, **(b)** $\Delta(\text{O}_2/\text{Ar})$, $p\text{CO}_2$, **(c)** Chl a, NCP and surface concentration of DIN along Transect 4 in June 2015. The plots of $\Delta(\text{O}_2/\text{Ar})$, $p\text{CO}_2$ and NCP are 10-point Savitzky-Golay smoothed.

900

901

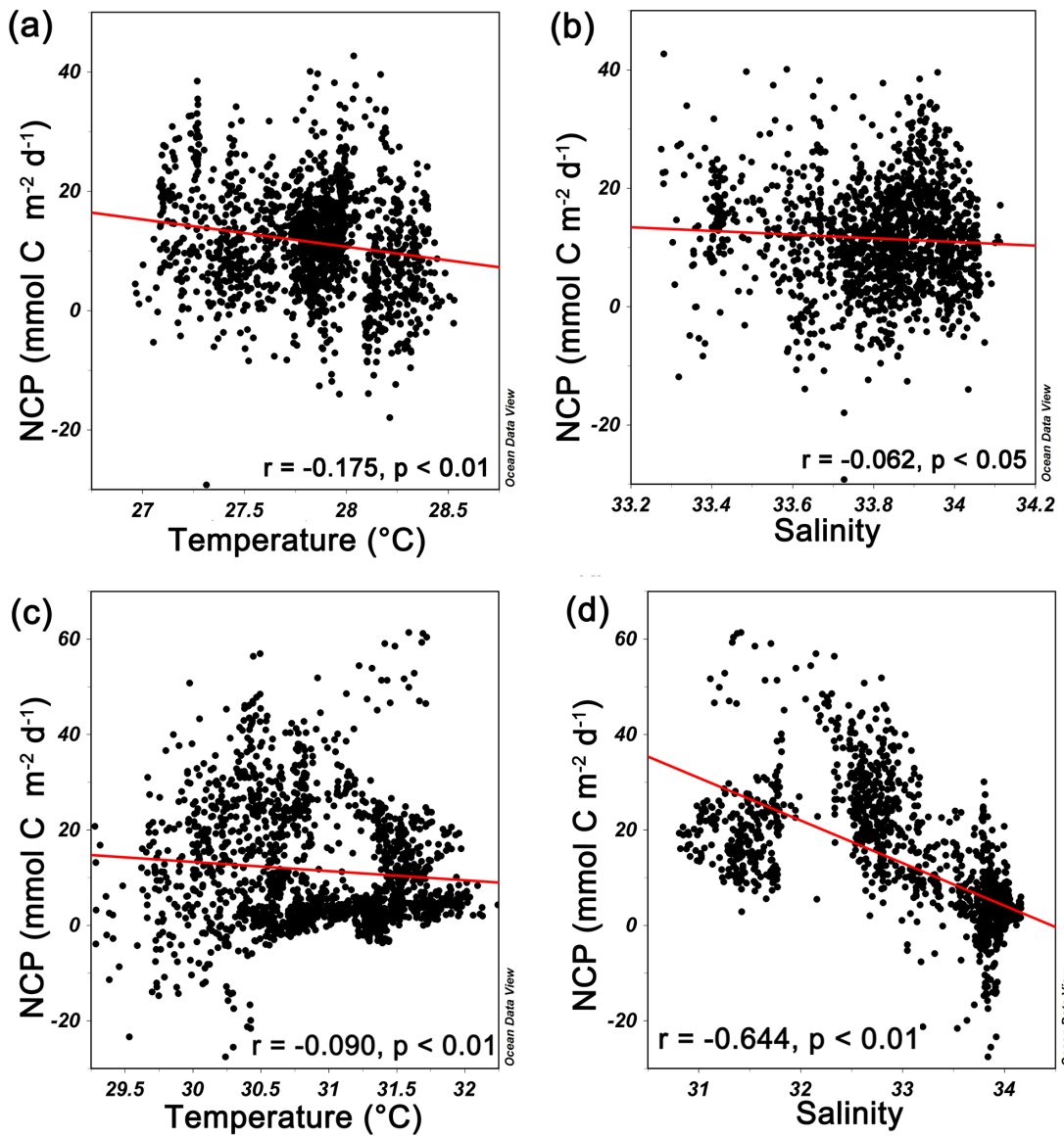


902 **Figure 7.** Principal Component Analysis (PCA) among variables for (a) October 2014 and (b) June 2015 (Bartlett's test of
 903 sphericity: $p < 0.01$)
 904
 905



906
907
908
909
910
911

Figure 8. (a) T-S diagram of surface DIN concentration in June 2015. The stations influenced by shelf water were in the red circle. (b) Correlation analysis between surface DIN concentration and NCP at sampling stations. The stations (characterized with $S < 33$) influenced by shelf water presented surface DIN concentration $\geq 0.27 \mu\text{mol L}^{-1}$.



912

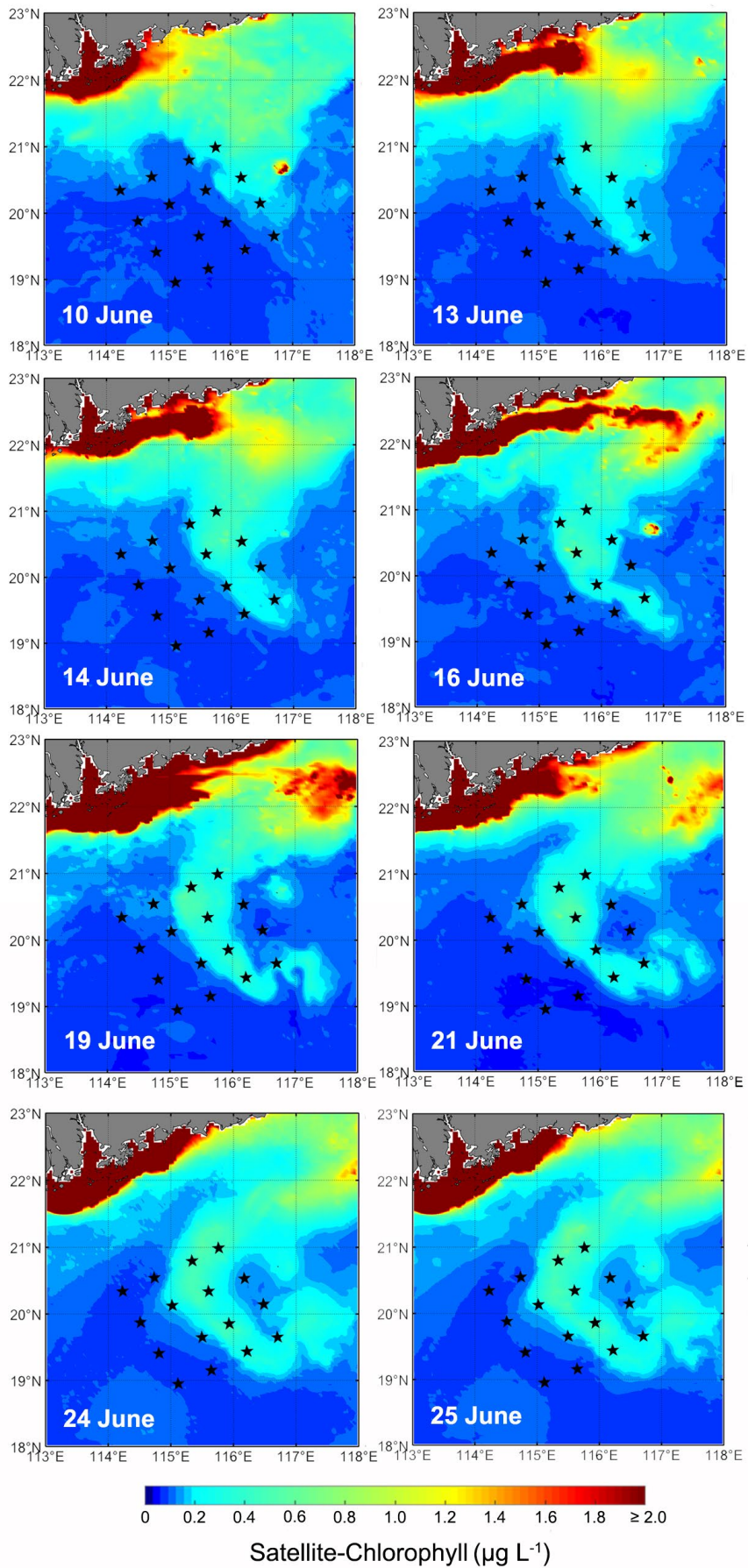
913

Figure 9. Correlation analysis between underway NCP and physical parameters (temperature and salinity) in October 2014

914

(a, b) and June 2015 (c, d).

915



916
917
918
919

Figure 10. Daily satellite-chlorophyll images on the selected days in June 2015. Stars represent CTD locations. We roughly set satellite-chlorophyll $\geq 0.2 \mu\text{g L}^{-1}$ in this figure as the criterion of shelf water. This figure was made based on the M_Map mapping package for MATLAB (Pawlowicz, 2020).